HHS Public Access

Author manuscript

Nat Biotechnol. Author manuscript; available in PMC 2024 July 17.

Published in final edited form as:

Nat Biotechnol. 2024 July ; 42(7): 1075–1083. doi:10.1038/s41587-023-01950-1.

A DNA nanodevice for mapping sodium at single organelle resolution

Junyi Zou[1,2], **Koushambi Mitra**[1,2], **Palapuravan Anees**[1,2], **Daphne Oettinger**[1,2], **Joseph Ramirez**[1,2], **Aneesh Tazhe Veetil**[1,2], **Priyanka Dutta Gupta**[1,2], **Rajini Rao**[3], **Jayson J. Smith**[2,4], **Paschalis Kratsios**[2,4], **Yamuna Krishnan**[1,2,5,*]

[1.]Department of Chemistry, The University of Chicago, Chicago, IL, USA.

[2.]Neuroscience Institute, The University of Chicago, Chicago, IL, USA.

[3.]Department of Physiology, Johns Hopkins University School of Medicine, Baltimore, MD, USA.

[4.]Department of Neurobiology, The University of Chicago, Chicago, IL, USA

[5.]Institute for Biophysical Dynamics, The University of Chicago, Chicago, IL, USA.

Abstract

Cellular sodium ion (Na^+) homeostasis is integral to organism physiology. Our current understanding of Na^+ homeostasis is largely limited to Na^+ transport at the plasma membrane. Organelles may also contribute to Na^+ homeostasis, however, the direction of Na^+ flow across organelle membranes is unknown because organellar Na^+ cannot be imaged. Here, we report a pH-independent, organelle-targetable, ratiometric probe that reports lumenal Na^+. It is a DNA nanodevice containing a Na^+-sensitive fluorophore, a reference dye and an organelle targeting domain. By measuring Na^+ at single endosome resolution in mammalian cells and in *C. elegans*, we discovered that lumenal Na^+ levels in each stage of the endolysosomal pathway exceed cytosolic levels and decrease as endosomes mature. Further, we find that lysosomal Na^+ levels in nematodes are modulated by the Na^+/H^+ exchanger NHX-5 in response to salt stress. The ability to image sub-cellular Na^+ will unveil mechanisms of Na^+ homeostasis at an increased level of cellular detail.

Cells move Na^+ across their plasma membrane and organelle membranes to regulate both cytosolic and organellar Na^+ and thereby maintain cellular Na^+ homeostasis. Organelle membranes account for ~95% of total membrane in the cell, yet most of our understanding of cellular Na^+ homeostasis relates to its movement across only 2–5% that comprises the plasma membrane[1]. Few lines of evidence suggest that organelles could contribute to the

* yamuna@uchicago.edu .

Author contributions

J.Z. and Y.K. designed every aspect of the study. K.M., A.T.V. and J.R. designed and synthesized the CG dye. J. Z. made, characterized, and validated *RatiNa* in vitro, in cells and *in vivo*. J.Z., and P.A. performed Na^+ measurements in worms. D.O. performed all the brood size experiments. P.A. performed pH measurements in worms. J.J.S. and P.K. made the NHX-5::GFP worm. P.D.G and R.R. provided NHE6 KO macrophages. J.Z. and Y.K. analyzed and interpreted all data. J.Z., K.M. and Y.K. wrote the paper. All authors provided input on the manuscript.

Competing interests

The authors declare no competing interests. YK is a co-founder of Esya Inc and MacroLogic Inc that use DNA nanodevices to develop diagnostics and therapeutics respectively.

mobilization and transport of Na^+ in single cells. Many endosomal Na^+/H^+ exchangers (NHEs) were first identified in yeast due to the lethality they caused upon salt stress when they were knocked out[2,3]. In humans, there are thirteen NHE proteins (NHE1–9, NHA1–2, SLC9C1–2) encoded by the *SLC9A-C* gene family[4,5]. NHE9 resides in late endosomes and is genetically linked to autism[6,7]. Loss of function mutations in NHE6, which resides in early and recycling endosomes, causes the X-linked neurological disorder Christianson's syndrome in humans[8]. In plants and fish, the loss of a vacuolar Na^+/H^+ exchanger (Nhx1) in Japanese morning glory or a lysosomal $Na^+/Ca^{2+}/K^+$ transporter (slc24a5) in zebrafish cause stark pigmentation phenotypes[9,10]. Apart from transporters, organelles have voltage-gated Na^+ channels[11–13] that are likely functional since many endocytic organelles were recently found to harbor high membrane potential[14]. Although extracellular and cytosolic Na^+ levels at the tissue and single cell levels are known[15,16], those within organelles are not. Consequently, the direction of ion flow across an organelle membrane cannot be predicted if a given organelle-resident Na^+ channel or transporter is activated and therefore we cannot predict how organelles might contribute, if at all, to cellular Na^+ homeostasis in health and disease.

Results

Organellar Na^+ levels have not been mapped because there are no probes that work in the acidic conditions of organelle lumens. All fluorescent Na^+ probes are acid sensitive because they detect Na^+ by coordination via protonatable groups[17]. Further, genetically encodable reporters of Na^+ do not exist. Hence, previous estimates of lumenal Na^+ relied on elemental analysis of isolated organelles or null point titration that averages the information from different organelles[18,13]. Given recent evidence of organelle subpopulations that differ either in lumenal ionic composition[19], metabolite content[20], or membrane potential[14] population-averaged measurements may mask the precise contribution of organelles to cellular Na^+ homeostasis[13,18].

Here, we have developed a pH-insensitive Na^+ reporter, denoted *RatiNa*, that can *rat*iometrically image *i*ntracellular *Na*$^+$ in single organelles in intact cells. *RatiNa* is a 45-base pair DNA duplex comprising three single-stranded DNA (ssDNA) molecules: a 25-mer strand carrying a Na^+ sensitive fluorophore for sensing (D1); a 45-mer strand bearing an ion-insensitive internal reference dye for ratiometry (D2), and a 20-mer strand harboring the targeting module that localizes *RatiNa* in the lumen of specific organelles (D3) (Fig. 1a).

Based on the sensing mechanism of the Na^+ probe, CoroNa Green[21], we synthesized a novel pH-insensitive fluorophore for D1, denoted Chicago Green (CG, λ_{ex} = 510 nm, λ_{em} = 530 nm) (Extended Data Fig. 1a, Supplementary Fig. 1, Note 1). Like CoroNa Green, CG binds Na^+ through a 1-aza-15-crown-5 ether moiety and uses photoinduced electron transfer (PET) to switch on or off fluorescence. Because fluoro substitutions generally lower the pK_a of fluoresceins[22], CG has a tetrafluoro fluorescein core to reduce its pH sensitivity. Hence CoroNa Green is pH sensitive because the aza-crown and hydroxyl groups are largely protonated at pH 4.5 while CG is not. CG is therefore suitable for organelles. We show the Na^+ binding affinity (K_d) of CG is pH independent between pH 4.5–7 (Extended Data Fig. 1b–c). CG is further modified with a propargyl group for conjugation to a 5'-azido

substituted D1 using copper-catalyzed azido-alkyne cycloaddition (Supplementary Fig. 2 – 3, Note 2)[23,24]. We chose ATTO647N (λ_{ex} = 646 nm, λ_{em} = 663 nm) as the reference dye on D2 because it is bright, photostable, and insensitive to pH, Na^+ and other ions[25]. Because its emission spectrum does not overlap significantly with CG, the ratio of CG (G) to ATTO647N (R) fluorescence (G/R) in *RatiNa* corrects for CG intensity differences arising from inhomogenous probe distribution and/or uptake[26]. This correction gives a readout for Na^+ concentration ([Na^+]) alone. When D3 hybridizes to D1 and D2, it forms a 45-bp duplex DNA that targets *RatiNa* to endocytic organelles via receptor mediated endocytosis (Supplementary Fig. 4, Note 3, Table 1)[27,28,29].

When attached to *RatiNa*, CG excitation and emission maxima were red shifted by ~12 nm but its intensity still increased with increasing [Na^+], while that of ATTO647N was constant (Fig. 1b –c). We calibrated *RatiNa* immobilized on streptavidin-coated beads by fluorescence imaging in buffers of varying pH and [Na^+] (Supplementary Fig. 5, Note 4). The three-dimensional surface plot of G/R values versus pH and [Na^+] shows that the Na^+ response of *RatiNa* is pH independent (Fig. 1d, Extended Data Fig.1d–f). Further, *RatiNa* response is specific to Na^+ and barely affected by other physiological ions like K^+, Li^+, Ca^{2+} and N-methyl-D-glucamine (NMDG) (Fig. 1e, Extended Data Fig. 1g). *RatiNa* showed a similar Na^+ response in buffers with a mixture of ions in proportions that matched either the extracellular or cytosolic milieu (Fig. 1e). Together, these data show *RatiNa* is pH-insensitive and specific enough to measure Na^+ in acidic organelles.

Given lysosomes are the only organelles with previous population averaged Na^+ measurements that can be used for validation[13,18], we used *RatiNa* to map lysosomal Na^+ in cultured murine macrophages and *in vivo* in coelomocytes of the nematode *C. elegans*. Both these systems are amenable to analysis with DNA nanodevices because they express scavenger receptors abundantly, whose cognate ligand is duplex DNA[28,29,30,]. To track *RatiNa* trafficking and determine when it reaches lysosomes in both systems, we used a *RatiNa* lacking CG and carrying only the ATTO647N dye (*RatiNa*^{AT}). We also used LMP1::GFP worms whose lysosomes are labeled with green fluorescence protein (GFP), and RAW 264.7 macrophages whose lysosomes are labeled with TMR dextran. In LMP1-GFP worms, *RatiNa*^{AT} colocalized with GFP-labeled lysosomes 1 h post-injection (Fig. 2a). Pulsing RAW 264.7 macrophages with 500 nM *RatiNa*^{AT} for 2 h followed by a 30 min chase led to robust colocalization with the TMR-labeled lysosomes. Because lysosomes of murine macrophages are more degradative than those in nematodes[31], we tested the stability of *RatiNa*^{AT} in macrophages and found that the fluorescence of *RatiNa*^{AT} was stable up to 3 h (Extended Data Fig. 2a–c, Supplementary Note 5). Thereafter, fluorescence decreases as *RatiNa*^{AT} progressively degrades thereby liberating the ATTO dye, which eventually leaches out of the lysosomes. Based on these results, we conducted all Na^+ measurements within 30 min of *RatiNa* labeling lysosomes.

We confirmed *RatiNa* response was not obscured by autofluorescence in worms or live cells. In the physiologically relevant regime of Na^+ (5 mM to 145 mM), the performance characteristics of *RatiNa* in both worms and live cells were similar to those on beads incubated in buffers of known pH and [Na^+] (Fig. 2b–d, Extended Data Fig. 2d–g). We calibrated *RatiNa* response by imaging *RatiNa*-labeled beads in increasing [Na^+],

and *RatiNa*-labeled worm lysosomes whose lumenal pH and Na^+ have been clamped using buffers of defined pH and [Na^+] containing a cocktail of ionophores[18,32] (Fig. 2c, Supplementary Note 6–7). Lysosomal G/R ratios increased linearly with [Na^+] whether *RatiNa* was in *C. elegans*, RAW 264.7 macrophages, or on beads, demonstrating that degradation, if any, is negligible under these conditions (Fig. 2d,).

To obtain Na^+ levels of single lysosomes, we generated heatmaps of Na^+ from the G/R images of *RatiNa*-labeled lysosomes in resting cells and compared them to the *in vivo* or *in cellulo* calibration profile as relevant (Fig. 2e, Extended data Fig. 2h). In both worms and RAW 264.7 macrophages, lysosomes Na^+ was surprisingly variable. Na^+ in single lysosomes ranged between 5 mM to 145 mM, averaging ~43 mM in *C. elegans* and ~48 mM in RAW 264.7 macrophages. Since *RatiNa* labeling bypasses the need to permeabilize cells[18] or purify lysosomes[13], it enables lysosomal Na^+ measurement under the most native conditions so far. Previous measures ranged from 20 mM[18] in macrophages to 150 mM[13] in HEK293T cells measured by different methods. Our measure of average lysosomal Na^+ compares better with that in macrophages, but our single lysosome measurement shows that lysosomes can harbor high Na^+, and lysosomal Na^+ likely varies across different species and cell types.

By mapping Na^+ as a function of endosomal maturation, we show that *RatiNa* can capture physiological differences in organellar Na^+. Because DNA nanodevices are internalized via scavenger receptors into early endosomes that mature to late endosomes and eventually lysosomes[33], *RatiNa* acts as an endocytic tracer, labeling each stage of endosomal maturation as a function of chase time post-injection (Supplementary Note 8). We determined these chase times by injecting *RatiNa*^{AT} into nematodes expressing either the early endosome marker, RAB-5[27], or the late endosome marker, RAB-7[27]. *RatiNa*^{AT} localized in early endosomes at 5 min and late endosomes at 17 min post-injection with negligible off-target labeling of other organelles on the endolysosomal pathway (Fig. 3a–b, Extended data Fig. 3a–b). When Na^+ in early endosomes and late endosomes was measured using *RatiNa* as described above for lysosomes, we found that lumenal Na^+ is highest in early endosomes (~74 mM) and drops to ~51 mM in late endosomes (Fig. 3c–d). The change in concentration was not due to overall differences in volume between EEs and LEs (Supplementary Fig. 6, Note 9). Notably, because every other ion mapped so far (*i.e.*, H^+, Cl^- or Ca^{2+}) increases progressively along the endolysosomal pathway[27,34,35], our data reveals that uniquely, Na^+ levels decrease as a function of endosomal maturation, implicating Na^+ efflux mechanisms every endosomal stage.

RatiNa could also capture physiological differences in Na^+ arising from the activity of a Na^+ channel or transporter in a specific organelle. Two-pore channel type 2 (TPC2) is a lysosomal membrane protein that can function as an NAADP activated Ca^{2+} channel[36] or a PI(3,5)P2 activated Na^+ channel[13]. We first tested whether *RatiNa* could capture changes in lysosomal Na^+ upon pharmacological perturbation of TPCN2. Torin-1 treatment is expected to activate TPCN2 because it inhibits mammalian target of rapamycin (mTOR), which in turn inhibits TPC2[12,37]. Indeed, treating RAW 264.7 macrophages with 1 μM Torin-1 for 1h lowers lysosomal Na^+ to ~22 mM (Fig. 3e). In contrast, treating RAW 264.7 macrophages with apilimod, a specific PIKfyve inhibitor[38] that depletes PI(3,5)P2 and blocks TPCN2,

elevated lysosomal Na^+ to ~70 mM (Fig. 3f). To specifically test the effect TPC2 activity on lysosomal Na^+ levels, we knocked out the *Tpcn2* gene in RAW 264.7 macrophages using CRISPR-Cas9 technology, confirmed by both genomic sequencing and qRT-PCR (Supplementary Fig. 7). Na^+ levels in lysosomes of *Tpcn2*$^{-/-}$ RAW 264.7 macrophages increased to ~67 mM, compared to ~43 mM in WT macrophages (Fig. 3g). Thus, as expected, ablating an organellar Na^+ channel elevates lumenal Na^+.

Next we tested whether *RatiNa* could be applied to study endosomal Na^+ transporters. NHE6 is an endosomal Na^+/H^+ exchanger[39] Mutations in NHE6 cause Christianson syndrome and these patients also show lysosomal disorder phenotypes[8]. Loss of NHE6 causes defects in endosome maturation and trafficking underlying lysosome deficiency[8]. We applied *RatiNa* in primary bone marrow derived macrophages from WT and *Nhe6*$^{-/-}$ mice. Because *Nhe6*$^{-/-}$ mice have defective endocytosis and trafficking, *RatiNa* required a 45 min chase to label lysosomes (Supplementary Fig. 8). We found that lysosomes in *Nhe6*$^{-/-}$macrophages showed higher WT, lysosomal Na^+ than in WT BMDMs (Fig. 3h) even though NHE6 is suggested to import Na^+ into endosomes. Loss of NHE6 is linked to endosomal trafficking defect and impaired delivery of functional proteins such as Cathepsin D to lysosomes[8]. It is possible that Na^+ could be elevated because the loss of NHE6 could impair the localization of lysosomal Na^+ channels.

We then used *RatiNa* to map Na^+ transport in lysosomes of *C. elegans* under salt stress. Excess salinity stresses many species, including *C. elegans*, by interfering with osmoregulation[40,41]. While salt stress has been studied at cellular resolution in whole animals[42], it is not known whether salt stress can impact sub-cellular Na^+ levels. *C. elegans* responds to salt stress by increasing glycerol and sorbitol synthesis and regulating its body volume[41,42]. We used a well-established assay[41] to acutely (Ac) or chronically (Ch) stress *C. elegans* to high Na^+ (Supplementary Fig. 9 and Supplementary Note 10). Briefly, worm eggs of the relevant genetic background were grown at either normal salt (50 mM NaCl, NS) or at elevated salinity (200 mM, Ac). Then, at the L4 stage larvae were transferred and grown in progressively higher levels of Na^+ (Ch) up to a maximum of 400 mM Na^+. Brood sizes at each salt concentration were measured and compared to those of unstressed worms (NS). At 400 mM Na^+, only chronically stressed wild type (N2) worms produced progeny (Fig. 4a, Extended Fig. 4a).

Mutant worms for various genes encoding Na^+/H^+ exchangers (NHX) proteins[43] did not reproduce at 400 mM Na^+ indicating intolerance to salt stress (Fig. 4b and Extended data Fig. 4a). We found that worms lacking *nhx-5*, which encodes the closest homolog to human NHE6[44], were the most severely affected, failing to produce progeny even at 300 mM Na^+. To pinpoint organelle participation in tolerating salt stress, we measured lumenal Na^+ in early endosomes (EE), late endosomes (LE), and lysosomes (LY) in *nhx-5(−)* mutants (Fig. 4c). While Na^+ levels in EE and LE of NHX-5 mutants were comparable to those in N2 worms, those in lysosomes were significantly lower. Lysosomal Na^+ in *nhx-7(−)* and *nhx-8(−)* mutants were not significantly altered, demonstrating that NHX-5 specifically facilitates lysosomal Na^+ import (Fig. 4d and Extended data Fig. 4b). NHX-8 and NHX-7 are the closest worm homologs of mammalian NHE8 and NHE2 that reside on the Golgi and plasma membrane, respectively[45,46]. We found NHX-5::GFP localizes in lysosomes of

coelomocytes (Supplementary Fig. 10, Note 11). Salt tolerance is compromised in worms lacking either plasma membrane or organellar Na^+ transporters, revealing that even in metazoans, organelles participate in Na^+ homeostasis (Supplementary Note 12).

When we mapped lumenal Na^+ along the endolysosomal pathway in chronically stressed N2 worms, we found Na^+ levels in EEs, LEs and LYs were all lowered. However, the effect was most pronounced in lysosomes, which showed ~67% decrease (Fig. 4e). Interestingly, in the few *nhx-5* mutants that survived chronic salt stress, Na^+ levels in EEs and LEs were similar to their unstressed counterparts. Yet, lysosomal Na^+ in chronically stressed *nhx-5(−)* mutants increased ~8-fold, despite no change in the corresponding mRNA levels (Fig. 4f, Extended data Fig. 4c). Lysosomal Na^+ mildly increases even in chronically stressed *nhx-7(−)*, *nhx-8(−)* or *ncx-2(−)* single mutants (Extended data Fig. 4d, Supplementary Note 12). Our data show that organelles modulate their Na^+ levels as worms are subjected to salt stress, with the biggest change occurring in lysosomes. These changes likely reflect both osmotic stress and Na^+ stress[47], which favour more inert osmolytes like glycerol over Na^+ in the worm body[41], and possibly also in the lysosome.

NHX family proteins are electroneutral transporters that work bi-directionally and can either import or export Na^+ in a 1:1 ratio with H^+ across membranes depending on cellular demand[48]. Therefore, to better understand the role of NHX-5 in lysosomes, we measured lysosomal pH in N2 and *nhx-5*(−) worms in unstressed and salt-stressed states (Extended data Fig 5a–d). Unstressed *nhx-5(−)* worms have less Na^+ and lower pH compared to N2 worms, suggesting that NHX-5 imports Na^+ using the pH gradient. Notably, the lysosomal pH change of 3 μM is eclipsed by the lysosomal Na^+ change of ~30 mM suggesting that the pH changes due to NHX-5 activity are likely compensated by highly active lysosomal V-ATPase[49]. Interestingly, salt stress too, has no effect on lysosomal pH in either genetic background, indicating the importance of directly mapping organellar Na^+ to study salt stress at the sub-cellular level.

To test the role of lysosomes in counteracting salt stress, we subjected a range of mutant nematodes, each lacking a specific lysosomal enzyme or transporter, to salt stress. Each mutant is a genetic model of a given lysosomal storage disorder caused by a lysosomal defect[50,51]. Many mutants were hypersensitive to chronic salt stress (Extended data Fig. 6a). Interestingly, worms lacking *slc38a9* were hypersensitive to acute salt stress (Extended data Fig. 6b). Human SLC38A9 is a lysosome-resident sodium-coupled neutral amino acid transporter which uses Na^+ to regulate nutrient transport, lysosome functionality and metabolism[52]. Although lysosomal Na^+ in *slc38a9(−)* worms and N2 worms is similar (~40 mM), acute salt stress elevates lysosomal Na^+ in *slc38a9(−)* worms, just as seen in chronically salt-stressed *nhx-5(−)* worms (Extended data Fig. 6c–d). These findings underscore a role for the lysosome in regulating salt stress.

Discussion

In summary, we present a pH-independent, ratiometric fluorescent probe that reports absolute Na^+ levels in acidic organelles with single organelle resolution. Using the probe, we found that unlike any other ion previously mapped on the endolysosomal pathway,

Na^+ levels decrease as endosomes mature. While average lysosomal Na^+ is comparable in both *C. elegans* and mammalian macrophages, the levels in single lysosomes varied considerably. Even within in the same cell, lysosomes vary in their morphology, mobility and function[19,53]. This variability is often under-appreciated in terms of ion composition. For example, we consider that H^+ levels are stringently regulated. Yet in an ensemble of lysosomes, pH routinely spans 4.4 – 4.6 i.e., 40 μM - 25 μM H^+, nearly 60% difference[28]. Lysosomal Ca^{2+} can vary from 5 μM – 300 μM, nearly 60-fold difference[28,35]. Thus, the heterogeneity of lysosomal Na^+ is commensurate with other ions. Our results show that at every stage of maturation, endosomes have both a sizeable transmembrane Na^+ gradient in addition to high membrane potential[14]. The progressively decreasing Na^+ level implicates the function of proteins that mediate Na^+ efflux at each stage of the endolysosomal pathway. While we know of only TPC2 as a bona fide lysosomal Na^+ channel[13,36], our findings suggest the existence of more endosomal Na^+ channels.

RatiNa can also capture physiological changes in lysosomal Na^+ levels due to the activity of Na^+ channels such as TPC2 or exchangers like NHE6. Given the ability to map organellar Na^+ fluxes *in vivo*, we found that NHX-5, facilitates lysosomal Na^+ import. When worms encounter salt stress, of all the organelles on the endolysosomal pathway, the biggest decrease in lumenal Na^+ occurs in the lysosome. Worms lacking lysosomal Na^+ transporters such as NHX-5 or SLC38A9 were highly susceptible to salt stress. The few mutants that survived salt stress showed abnormally high Na^+ in their lysosomes. Further, worms with specific lysosomal defects were hypersensitive to salt stress, positioning lysosomes as a critical conduit for Na^+ homeostasis in metazoans.

While vacuolar Na^+/H^+ exchangers regulate cytosolic pH and Na^+ levels in yeast during salt stress[3] and help counter hypotonic stress in cultured mammalian cells[54,55], the direction of Na^+ flux across organelle membranes was unknown. Our results indicate that in unstressed worms, NHX-5 imports Na^+ into and extrudes H^+ from lysosomes. However, the low level of lysosomal Na^+ in *nhx-5(−)* worms under salt stress points to more complex mechanisms of lysosomal Na^+ regulation. The minimal change in lysosomal pH under salt stress suggests that lysosomal Na^+ is likely regulated by players other than NHX-5. A probe like *RatiNa* can potentially be used to identify more players.

To survive high Na^+ stress, cells must undergo a metabolic shift[56] to produce organic osmolytes such as sorbitol to increase the internal osmotic pressure[57]. Cells upregulate autophagy[58] and lysosomal proteolysis to generate and recycle nutrients that are substrates for osmolyte production pathways. The metabolic shift is supported by numerous nutrient transporters that move these substrates across lysosomal and plasma membranes into the cytosol[59]. Many nutrient transporters move their substrates across membranes by co-transporting Na^+ and thereby leveraging the transmembrane Na^+ gradient[52]. Many nutrient transporters and their regulators, such as mTOR, reside on the lysosomal membrane[60,61]. Thus, lysosomes are a hub that supports this metabolic shift[62]. This provides a rationale for the large Na^+ flux across lysosomes during salt stress. While in higher organisms we know of Na^+ channels such as TPC2 that regulate organellar Na^+ homeostasis, none are known in *C. elegans*. Our ability to map organellar Na^+ *in vivo* can illuminate mechanisms of Na^+ homeostasis at an increased level of cellular detail.

Methods

Reagents.

All oligonucleotides (Supplementary Table 1) were high performance liquid chromatography (HPLC) purified and purchased from Integrated DNA Technologies (USA). They were subjected to ethanol precipitation and quantified by UV absorbance. ^{1}H NMR and ^{13}C NMR spectra of the newly compounds were recorded on a Bruker AVANCE II+, 500 MHz NMR spectrophotometer in $CDCl_3$ and tetramethylsilane was used as an internal standard. Mass spectra were recorded with an Agilent 6224 Accurate-Mass time-of-flight liquid chromatography–mass spectrometry. Streptavidin-coated microspheres were purchased from Bangs Laboratories, Inc., Gramicidin, nigericin, and monensin were purchased from Cayman Chemicals. All other reagents were purchased from Sigma-Aldrich (USA).

Conjugation of CG to DNA

5'-amine modified single strand DNA (IDT) was reacted overnight with 20 equivalents azide-$(PEG)_4$-NHS ester (Click Chemistry Tool, AZ103) in 100 mM Na_2HPO_4 buffer with pH adjusted to ~8.5 by adding $NaHCO_3$. DNA was ethanol precipitated for purification.

To test conversion of amine to azide, a small aliquot of azide-DNA was reacted with 2 equivalents 5kDa mPEG-DBCO (Nanocs, PG1-DB-5K) in 50 mM pH 7.0 phosphate buffer and run on 12% native PAGE. PEGylated DNA shows a gel shift and no azide-DNA band is seen.

CuAAC reaction was used to conjugate CG to azide-DNA. Copper catalyst was prepared by premixing $CuSO_4$ and THPTA (100 mM, 10 eq.). Azide-DNA (1.3 mM, 1 eq.) was purged with nitrogen for 1 min, and added to propargyl-CG (2.6 mM in DMSO, 2 eq.), $CuSO_4$/THPTA mix, and sodium ascorbate (1 M, 40 eq.) fully dissolved in 30% DMSO in buffer. The mixture was purged with N_2, the tube was sealed and equilibrated for > 5 h. DNA was precipitated and analyzed by 12% native PAGE and UV-Vis. UVP VisionWorksLS v8.1.2 and Image Lab Software 6.0.0 was used for UV and fluorescence of gel imaging. Shimadzu UVProbe v2.43 software was used for UV-Vis absorbance aquisition.

Na^+ sensitivity by fluorescence spectroscopy

100 nM of *RatiNa* was taken in UB buffer (10 mM HEPES, MES and KOAc, 140 mM NaCl/KCl). pH adjusted by HCl or KOH) and fluorescence emission spectra recorded in a Fluoromax (Horiba). Horiba FluorEssence v3.5.8.63 software was used for acquisition with following collection parameters: For CG, λ_{ex} = 522 nm, emission range 530 – 600 nm. For ATTO647N, λ_{ex} = 645 nm, emission range 660 – 700 nm.

RatiNa^{biotin} conjugation to streptavidin coated beads

1 μm streptavidin-coated polystyrene bead (Bangs Laboratories, CP01004) were washed twice with 50 mM pH 7.4 phosphate buffer by centrifuging at 4,000 xg and incubated with 10 μM of *RatiNa^{biotin}* in 50 mM potassium phosphate buffer, pH 7.4 with agitation for good

mixed. After 2 h the beads were recovered by centrifuging at 4,000 xg and stored in 50 mM potassium phosphate buffer, pH 7.4. with 0.1% of Tween-20 to prevent bead aggregation.

Na^+ sensitivity by bead imaging

RatiNa beads were resuspended in clamping buffer (1 mM to 2 M NaCl, 10 mM HEPES, 10 mM MES, 10 mM KOAc) with varying concentrations of [Na^+] (1 mM to 2 M) and pH (4.5–7.5). Beads were drop casted on poly-D-lysine coated glass bottom dishes (Cellvis D35–14) and imaged by wide field (Olympus IX83) or confocal microscopy (Leica Stellaris 8). Individual beads were analyzed from intensities in CG and ATTO channels. Average G/R for >100 beads were calculated and normalized to the lowest average G/R in all samples.

Na^+ selectivity by bead imaging

To assay *RatiNa* ion selectivity, *RatiNa*-coated beads were resuspended in 5 mM Na^+ buffer (5 mM NaCl, 10 mM HEPES, 10 mM MES, 10 mM KOAc, pH 7.4) and images acquired in both CG (G) and ATTO (R) channels in a widefield microscope. Then one of the extra cations or osmolyte (145 mM NaCl/ 145 mM KCl / 10 mM LiCl / 10 mM $CaCl_2$ / 10 mM $MgCl_2$ / 300 mM NMDG) was added to reach the indicated concentration. To assay *RatiNa* selectivity in a mixture of ions, *RatiNa*-coated beads were suspended in either 5 mM Na^+ or 145 mM Na^+ containing extracellular buffer (EB: 10 mM KCl, 0.1 mM $MgCl_2$, 10 mM $CaCl_2$, 10 mM HEPES, 10 mM MES, 5 mM glucose, pH = 7.4) or intracellular buffer (IB: 145 mM KCl, 10 mM $MgCl_2$, 0.1 mM $CaCl_2$, 10 mM HEPES, 10 mM MES, 5 mM glucose, pH = 7.4) respectively. Beads were imaged, and G/R values were calculated. The fold change in G/R was calculated from the G/R ratio after and before adding the cations/osmolytes. The values are represented as fold change of of 5 mM to 145 mM Na^+.

Colocalization Analysis

Pixel based colocalization PCC is not suitable for *C. elegans* because endosomes are too large. Hence the percentage of DNA containing compartments that also have a membrane marker is used to quantify targeting specificity. In RAW macrophages, lysosomes are smaller and a pixel-based PCC analysis is used instead. ImageJ plugin Coloc-2 was used for PCC analysis.

Na^+ clamping in *C.elegans*

For *C. elegans*, the Na^+ clamping buffer has a pH of 5.5 and contains 150 mM Na^+ and K^+, 150 mM Cl^-, 50 μM monensin, 50 μM nigericin, 10 μM gramicidin, 100 μM ouabain. 2 μM *RatiNa* is microinjected in *C. elegans* and after 30 min it labels endolysosomes in coelomocytes. A few perforations are introduced in worms, they are soaked in clamping buffer and imaged after 1 h.

Fluorescent microscopy of Imaging *RatiNa*

We used Olympus IX83 with metal halide lamp (X-cite 120Q), 60x objective (Olympus PlanApo N 60× 1.42 NA) and Photometric Evolve delta EMCCD camera. Acquisition was performed with Metamorph Premier v7.8.12.0 software. For CG channel we use 525/30 BP (Semrock FF01–525/30–25) as excitation filter, 532 nm dichroic mirror (Semrock Di02-

R532–25×36) and 575/40 BP (Chroma ET575/40m) as emission filter. For ATTO647N channel we use 640/30 BP (Chroma ET640/30x) as excitation filter, tri-band dichroic mirror (Chroma 89016bs) and 705/72 BP (Chroma ET705/72m) as emission filter.

We used Leica Stellaris 8 for confocal microscopy. White laser was set to 85% and 63x objective (Leica HC PL APO CS2 63× 1.40NA) and Hybrid detectors (Leica HyD X) were used. Acquisition was performed with Leica LAS X 3.7.4.23463. Sequential scan is used, with 95.5 μm pinhole. For CG 522 nm laser was used (30% and 10% intensity for macrophages and *C. elegans* respectively). Emission was collected from 530 – 580 nm (HyD X2 Gain 100). For ATTO647N, 646 nm laser was used (2% intensity) and emission collected from 655 – 780 nm (HyD X4 Gain 10).

Image analysis

All image processing is performed with ImageJ[4]. For *RatiNa* beads, binary images were thresholded in the ATTO channel. Single beads in focus are automatically picked by "Analyze Particles" plugin in ImageJ with circularity >0.8. Rolling ball method was used for background subtraction. G/R value of each bead is obtained from the ratio of integrated intensity in CG and ATTO channels. For *C. elegans*, endosomes and lysosomes are selected manually in ATTO channel. Rolling ball method was used for background subtraction. G/R value of each endosome or lysosome is calculated as above. For RAW macrophages, bright puncta corresponding to lysosomes are selected as ROI in images. Rolling ball method was used for background subtraction. G/R value of each lysosome is calculated as above.

Na^+ heatmap is generated from background subtracted images in CG and ATTO channels. Linear fit equation of G/R to Na^+ is applied using both images. The resulting image was pseudo coloured with Vridis lookup table.

Cell culture

WT and *Tpcn2*$^{-/-}$ RAW 264.7 macrophages (ATCC, TIB-71) were grown in DMEM medium (Gibco, 11995) with 10% heat inactivated FBS (Gibco, 26140) and 100 U/mL Pen Strep (Gibco, 15140), maintained at 37 °C in a humidified chamber in 5% CO_2. All the experiments were performed on cells >24 h post-passaging, at confluency ~50%.

RAW cell stability assay

Lysosomes are labeled with first with TMR-dextran (1 mg/mL TMR dextran with 1 h pulse and 16 h chase) and then with *RatiNa*^{AT} (2h pulse of 500 nM) The ratio of ATTO647 to TMR (R/G) intensities indicates ATTO signal loss due to DNA degradation. Cells are imaged at indicated chase times by wide field microscopy and R/G values calculated at each time point[5]. DNA degradation is tracked from the average R/G at each time point normalized to the 30 min chase time where it is undegraded.

Na^+ clamping in RAW 264.7 macrophages

Cells are pulsed with 1 μM *RatiNa* for 2 h and chased for 30 min to label lysosomes. Cells with *RatiNa* labeled lysosomes were treated with culture medium containing ionophores, to clamp organellar Na^+, washed with clamping buffer twice, incubated in Na^+ clamping

buffer for 1h at RT and then imaged. Na^+ clamping buffers (150 mM NaCl/KCl, 1 mM $CaCl_2$, 1 mM $MgCl_2$, 10 mM HEPES, 5 mM glucose, pH 5.5) recapitulate cell internal osmotic pressure (321 Osm) to prevent lysosome volume changes due to ion exchange. 50 μM monensin, 50 μM nigericin, 10 μM gramicidin are used as Na^+ and K^+ ionophores to clamp Na^+ and K^+ and 100 μM of ouabain is used to inhibit Na^+/K^+ ATPase and facilitate clamping.

Lysosome targeting in RAW 264.7 macrophages.

RAW 264.7 macrophage were pulsed with 0.5 mg/mL TMR dextran for 1 h in Opti-MEM (Gibco, 31985070) chased for 16 h in complete DMEM to label lysosomes. 1 μM *RatiNa*^{AT} was pulsed for 2 h in Opti-MEM and chased for 30 min in complete DMEM. Live cells were then imaged in FluoroBrite (Gibco, A1896701) with confocal microscope (Leica Stellaris 8) in TMR and ATTO channels.

Pharmacological inhibition

RAW 264.7 macrophages were treated with either 100 nM apilimod for 1 h or 1 μM Torin-1. Lysosomes were labeled as mentioned with *RatiNa* containing 100 nM apilimod or 1 μM Torin-1 in the chase and imaging media.

CRISPR KO of *Tpcn2* in RAW 264.7 macrophages

Tpcn2$^{-/-}$ RAW 264.7 macrophages were obtained from Creative Biogene (NY, USA). Briefly lentiviral transduction of Cas9 and sgRNA was used to specifically knock out mouse *Tpcn2*. The sgRNA sequence 5'-CATGGATGCTGGTTCATTGT-3' targeted exon 3 of mouse *Tpcn2*. Single clones were picked and genomic sequence and qRT-PCR confirmed KO of *Tpcn2* gene.

C. elegans strains and maintenance

Standard methods were followed for the maintenance of *C. elegans*. Wild type strain used was *C. elegans* isolated from Bristol (strain N2). Mutant strains were provided by the CGC, which is funded by NIH Office of Research Infrastructure Programs (P40 OD010440).

cdIs131 [pcc1::GFP::rab-5+unc-119(+)+myo-2p::GFP], a transgenic strain that expresses GFP-fused early endosomal marker RAB-5 inside coelomocytes.

cdIs66 [pcc1::GFP::rab-7+unc-119(+)+myo-2p::GFP], a transgenic strain that expresses GFP-fused late endosomal/lysosomal marker RAB-7 inside coelomocytes.

pwIs50 [lmp-1::GFP+Cbr-unc-119(+)], a transgenic strain expressing GFP-tagged lysosomal marker LMP-1.

nhx-5(ok661) is a deletion mutant with 1411 bp deletion in *nhx-5* gene (F57C7.2) and referred to as *nhx-5(−)* elsewhere.

nhx-7(ok583) is a deletion mutant with 1702 bp deletion in *nhx-7* gene (K09C8.1) and referred to as *nhx-7(−)* elsewhere.

nhx-8(ok549) is a deletion mutant with 1584 bp deletion in *nhx-8* gene (Y18D10A.6) and referred to as *nhx-8(−)* elsewhere.

ncx-2(gk879849) is a substitution mutant of R634 to stop codon in *ncx-2* gene (C10G8.5) and referred to as *ncx-2(−)* elsewhere.

gba-3(gk502826) is a substitution mutant of Q89 to stop ccodon in gba-3 gene (F11E6.1) and referred to as *gba-3(−)* elsewhere.

XT7 *(cln-3.2(gk41) I; cln-3.3(gk118) cln-3.1(pk479) V)* is a triple deletion mutant of all 3 *cln-3* genes (C01G8.2, ZC190.1.1., F07B10.1), referred to as *cln-3.2(−); cln-3.3(−) cln-3.1(−)* elsewhere.

clh-6(ok791) is a deletion mutant for cln-6 gene (R07B7.1) and referred to as *cln-6(−)*.

ctns-1(ok813) is a deletion mutant with 1942 bp deletion in ctns-1 gene (C41C4.7) and referred to as *ctns-1(−)* elsewhere.

slc38a9(syb6822) is a deletion mutant with 994 bp deletion in F13H10.3a gene generated with CRISPR-Cas9 at SunyBiotech. This mutant is referred to as *slc38a9(−)* elsewhere.

qRT-PCR

For *C. elegans*, total RNA was isolated from >50 young adult worms with Trizol. cDNA was synthesized with Maxima H Minus cDNA synthesis master mix (Thermo, M1661) according to manufacturer's protocol. qPCR was performed with Roche LightCycler 96. $\Delta\Delta C_T$ was used to calculate fold change difference of RNA level compared to control gene *act-1*. Following primers were used for qRT PCR:

nhx-5 fwd: CGT CAA CTG TAG CAG GTT CTA A

nhx-5 rev: GGA AAC GTA GGT GAG GAG TAT G

nhx-7 fwd: GGA GCT TTA CCA CAC GAC TTA T

nhx-7 rev: GTG CAT GAG CTG ACG AAT AGA

nhx-8 fwd: CCA TCG TTC AAC TCG TTA CCT

nhx-8 rev: GAG CAA TGC ACT CAA CAA TCC

ncx-2 fwd: GAT TGA TCG GAG GAG GAG ATA TTG

ncx-2 rev: GTA GTG AGC TGG ATC CAA GAA G

act-1 fwd: CGA GCG TGG TTA CTC TTT CA

act-1 rev: CTT CTG CAT ACG ATC AGC AAT TC

For RAW 264.7 macrophages, total RNA was isolated from cells from a single well from a 6 well plate. Trizol (Thermo) extraction, cDNA synthesis and qPCR was performed similar to worm. *Gapdh* was used as reference gene. Following primers were used for qRT PCR.

Gapdh fwd: AAG CTC ATT TCC TGG TAT GAC A

Gapdh rev: CTT GCT CAG TGT CCT TGC TG

Tpcn2 fwd: GGA GAC TGG TAT TGG GGC TT

Tpcn2 rev: CAA TGC TGG CTG ATG AGT TC

C. elegans targeting and colocalization

For colocalization assays, worms with fluorescent marker for early endosome, late endosome or lysosome are microinjected with 1 μM of *RatiNa*^{AT}.(8). Worms were transferred to fresh NGM plate after injection and imaged by confocal microscopy at 5 min, 17 min and 60 min to assess targeting to early endosomes, late endosomes and lysosomes respectively. Anti-colocalization was performed similarly. Targeting was evaluated as previously specified here.

NHX-5::GFP overexpression in *C. elegans*

NHX-5::GFP plasmid (pFH6) was gifted by Prof. Keith Nehrke from University of Rochester Medical Center[9]. It contains genomic sequences of *nhx-5* and 1.5 Kb of upstream promoter sequences. EGFP with synthetic intron was fused to the C-terminus. Transgenic animals carrying an extrachromosomal *Pnhx-5::NHX-5::GFP* array were generated by microinjecting the plasmid (100 ng/μL) into the gonads of adult hermaphrodites with the *myo-2::mCherry* plasmid (2 ng/μL) as a co-injection marker at a final total DNA concentration of 100 ng/μL. The presence of the extrachromosomal array was confirmed by pharyngeal mCherry fluorescence and F1 progeny was picked for *RatiNa*^{AT} colocalization.

C. elegans salt stress assay

C. elegans was stressed by salt using previously published protocol[10]. Briefly, high Na^+ containing plates were made by supplementing NaCl to NGM plate with either 200 mM, 300 mM or 400 mM NaCl). High Na^+ plates were sealed with parafilm and kept at 4 °C until needed. For chronic salt stress (Ch), gravid worms were transferred to 200 mM Na^+ plate and hatched worms were allowed to grow on 200 mM Na^+ plate for chronic salt stress. For acute salt stress (Ac), L4 worms were directly transferred from NGM plates to 200 mM, 300 mM or 400 mM NaCl plates.

To assay brood size, 5 Ch worms and Ac worms are transferred to 200 mM, 300 mM and 400 mM Na^+ plate at L4 stage. Worms laid egg for 24 h, removed from the plate, but progeny allowed to grow for another 48 h. Plates were photographed and brood size was counted.

C. elegans coelomocyte lysosomal pH measurement

pH of *C. elegans* was measured with our previously published DNA-based sensor *Bromo I-switch*[11]. Briefly, *Bromo I-switch* was made by annealing component strands and calibrated from fluorescence intensity ratio of D/A signals from pH 4.0 to 7.0. Next *in vivo* pH clamping was performed by injecting Bromo I-switch and perforating worms with clamping buffers of desired pH (10 mM HEPES, 10 mM MES, 10 mM NaOAc, 140 mM KCl, 5 mM NaCl, 1 mM $MgCl_2$, 2 mM $CaCl_2$) contaning 50 μM nigericin and 50 μM monensin. The *in vivo* clamped D/A data and *in vitro* calibration curve was used to generate the *in vivo* calibration curve. pH was measured by injecting worms with *Bromo I-switch*, a chase for 30 min followed by imaging with widefield microscope.

Mouse BMDM isolation

Homozygous male and female *Nhe6* (*slc6a6*) KO mice were obtained from Dr. Rajini Rao's laboratory at Johns Hopkins University[12], and rederived at the University of Chicago[13]. These mice were generated via insertion of the LacZ-Neo reporter gene encoding for β-galactosidase in the genomic locus of *Slc6a6*. The presence of the LacZ-Neo at this site added a stop codon and a polyadenylation termination signal which halted the transcription of the target gene resulting in the deficient mice. The tails clippings from the homozygous *Nhe6* deficient male and female mice and the litters were used for genotyping as per procedure outlined by Strømme et al[13]. The mice were housed, fed a standard diet and maintained at the animal facility. For bone marrow derived macrophages[14] the femur and tibia of the homozygous KO and WT female littermates were collected under sterile conditions and then differentiated for 7 days in culture media (1X DMEM supplemented with 10% fetal bovine serum, 1% Penicillin/Streptomycin and 0.002% prophylactic Plasmocin) containing recombinant murine M-CSF (10–20 ng/ml). The differentiated adherent macrophages were used for outlined assays. All procedures were conducted in compliance with Institutional Animal Care and Use Committee (IACUC) and Animal Resource Center (ARC) at University of Chicago.

Data analysis

Numerical data was processed and plotted with OriginPro 2023 10.0.0.154. For Na^+ measurement of cultured cells and C. elegans, MATLAB R2018a and ImageJ 1.53t was used for endosomal ROI picking and analysis respectively.

Extended Data

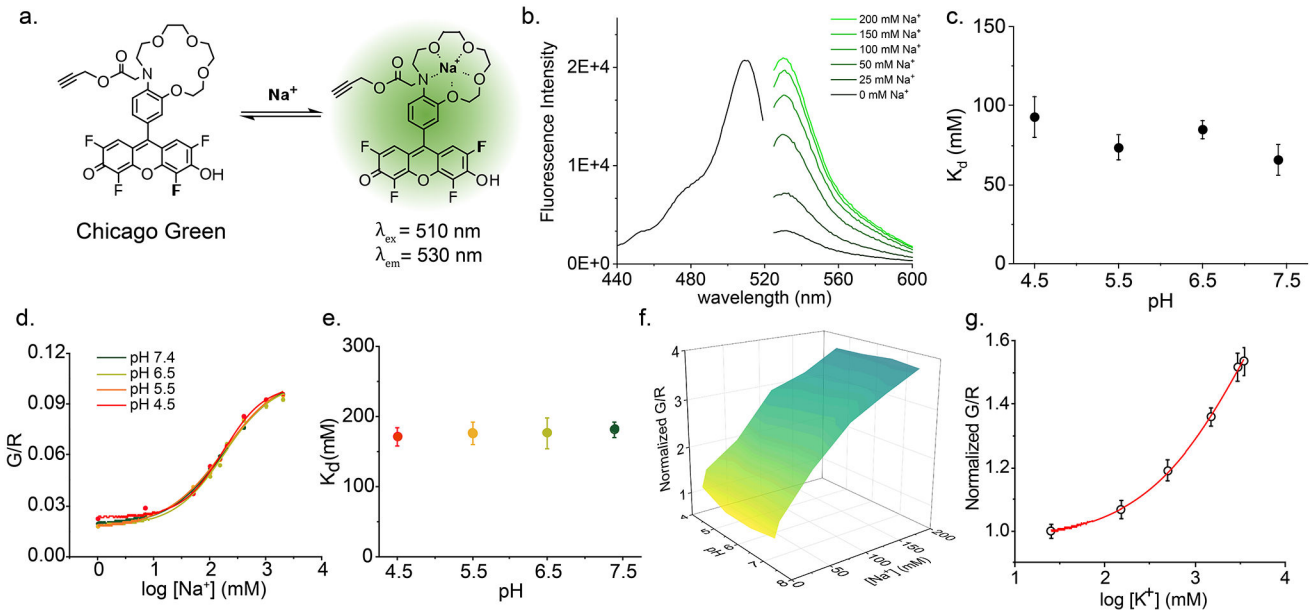

Extended Data Fig 1 |. Chicago Green (CG) is pH insensitive and selective to Na^+ prior to incorporation into *RatiNa*.

a, Na^+ sensing mechanism of CG **b**, Excitation (black) and emission (green) spectra of free CG increases with increasing Na^+. **c**, Dissociation constant (K_d) of CG for Na^+ does not vary with pH from pH 4.5 – 7.4 **d**, Individual *in vitro* calibration profiles of *RatiNa* at different pH in Fig. 1d. **e**, K_d of *RatiNa* for Na^+ at different pH values as calculated from **d**. K_d of *RatiNa* is higher than that of CG but is still pH invariant from pH 4.5 – 7.4. **f**, *RatiNa* response to K^+ yields a K_d of 4.5 M and 27-fold selectivity for Na^+ over K^+. **g**, Magnified view of *RatiNa* Na^+ calibration profile from 1 mM to 200 mM Na^+.

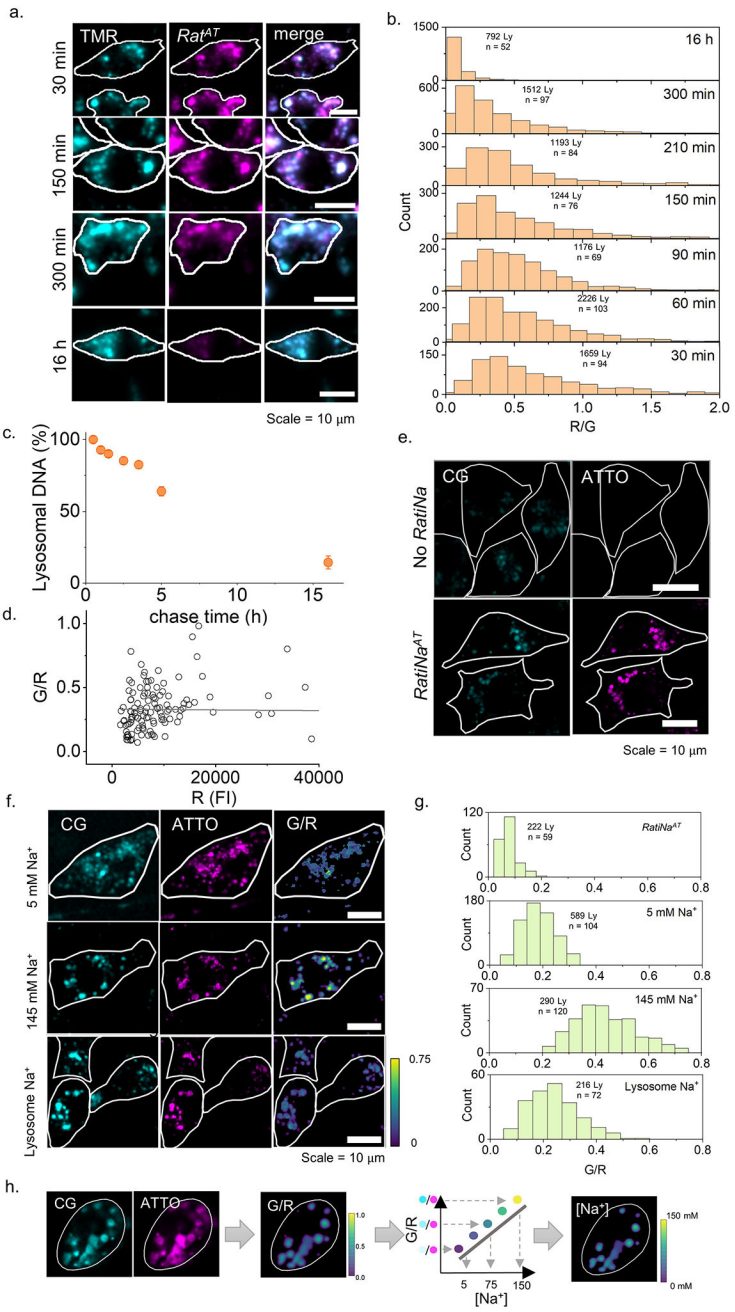

Extended Data Fig 2 |. Calibration of *RatiNa* and its stability in lysosomes of RAW264.7 macrophages.

a, Lysosomes in RAW264.7 macrophages prelabeled with TMR-dextran (cyan) and imaged at different chase times of *RatiNa*^{AT} (magenta). b, Histogram of single lysosome signal ratio of RatiNa^{AT}/TMR-dextran (R/G) at different chase time. A decrease of R/G indicates DNA degradation in lysosome over time. c, DNA degradation as a function of chase time calculated from b. Note that for 30 min chase time DNA is intact and ratiometry is valid. Error bar represents standard deviation. d, Normalized *RatiNa* signal (G/R) of single lysosome in RAW macrophage are plotted against the normalizing dye signal (R). The PCC analysis shows no correlation between G/R and R, indicating *RatiNa* signal and Na^+

measurement is independent of probe concentration. e, Fluorescence images of *RatiNa*^{AT} labeled RAW264.7 macrophages in CG (G) and ATTO (R) channels. Low amount of autofluorescence can be detected in the CG channel. f, Images of *RatiNa*-labeled lysosomes clamped at high and low Na^+ of 145 mM and 5 mM in native lysosomes. G/R heat maps show adequate change that Na^+ can be measured in native lysosomes.g, Histogram of G/R values of *RatiNa*-labeled single lysosomes. Accounting for autofluorescence represented by G/R in *RatiNa*^{AT} sample, the fold change in G/R signal of *RatiNa* in lysosomes of RAW264.7 macrophages is comparable to that in *C. elegans* and on beads. h, Schematic of workflow from raw images to Na^+ heat maps of single organelles. Fluorescent images in the CG (G) and ATTO (R) channels are used to construct the G/R image. Then the Na^+ heatmap was generated from the calibration curve of G/R to [Na^+].

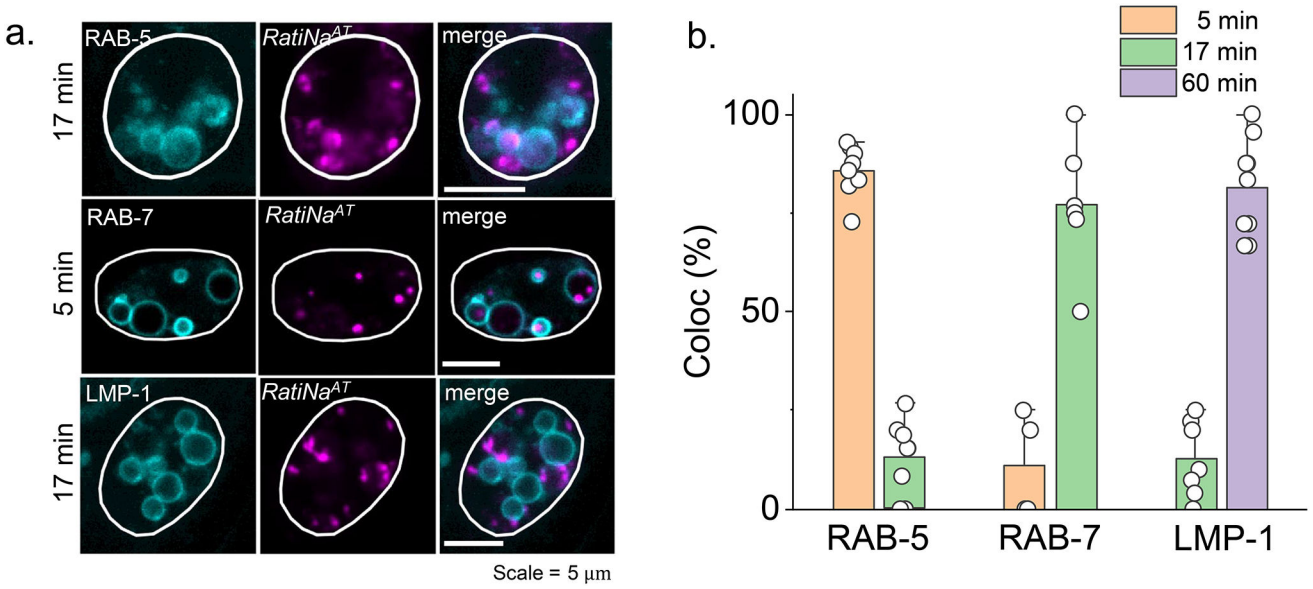

Extended Data Fig 3 |. Specificity of *RatiNa* targeting to endocytic organelles.

a, Representative images of *C. elegans* coelomocytes reveal negligible off-target labeling between *RatiNa*^{AT} and indicated endocytic markers and chase times. b, *RatiNa* is targeted to a specific endocytic organelle at fixed chase time. Colocalization is calculated as percentage of organelles having both lumenal *RatiNa*^{AT} and membrane marker fluorescence over all *RatiNa*^{AT} containing organelles (n = 9 coelomocytes of 6 worms in 5 min chase of RAB-5::GFP, 7 coelomocytes of 6 worms in 17 min chase of RAB-5::GFP, 4 coelomocytes of 4 worms in 5 min chase of RAB-7::GFP, 6 coelomocytes in 5 worms of 17 min chase of RAB-7::GFP, 7 coelomocytes in 6 worms of 17 min chase of LMP-1::GFP, 9 coelomocytes in 6 worms for 60 min chase of LMP-1::GFP)

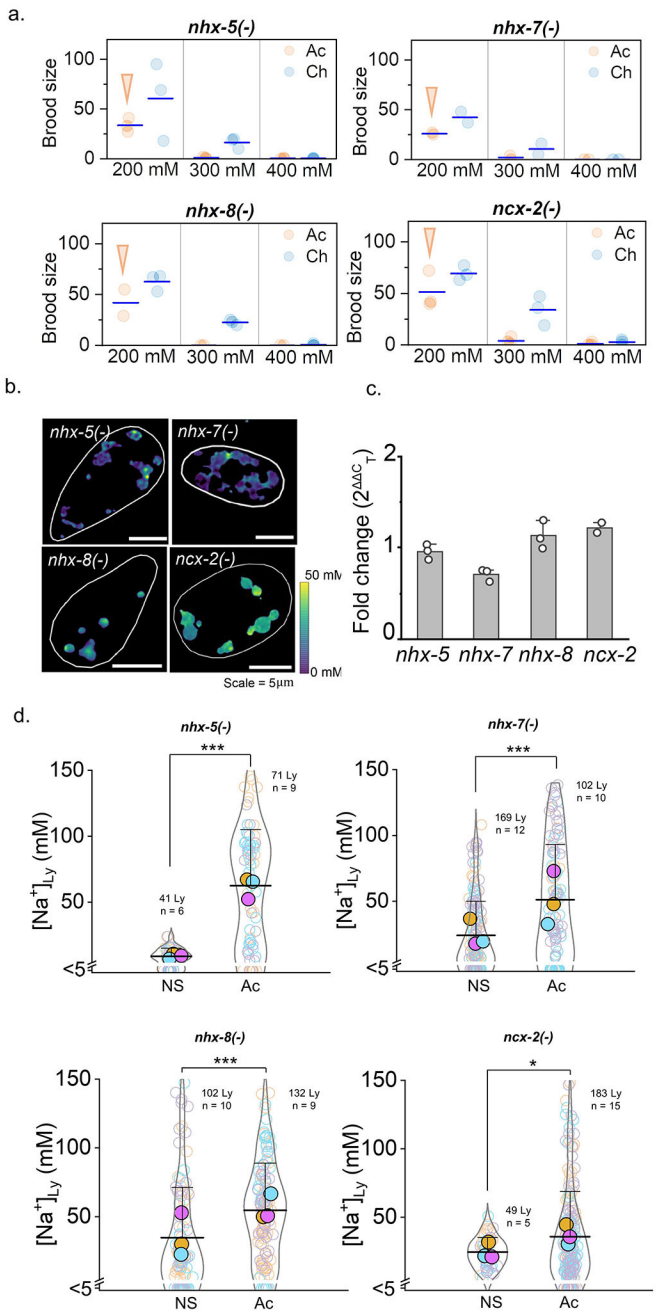

Extended Data Fig 4 |. *RatiNa* reports lysosomal Na^+ changes with inhibition of TPC2 and mTOR.

a, Apilimod is a strong inhibitor of PIKfyve that phosphorylate PI3P to PI(3,5)P2, which activate TPC2 channel to export lysosomal Na^+. Inhibiting PIKfyve causes less efflux of lysosomal Na^+. Lysosomal Na^+ increases from 39 mM in vehicle to 68 mM in 100 nM apilimod treated RAW macrophages. **b**, Torin-1 inhibits mTOR and induces autophagy. After acute 1 h treatment of 1 uM Torin-1, lower lysosomal Na^+ of 22 mM is observed compared to 40 mM in vehicle. *P ≤ 0.05; **P ≤ 0.01; ***P ≤ 0.001; ns, no statistical significance by two sample *t*-test.

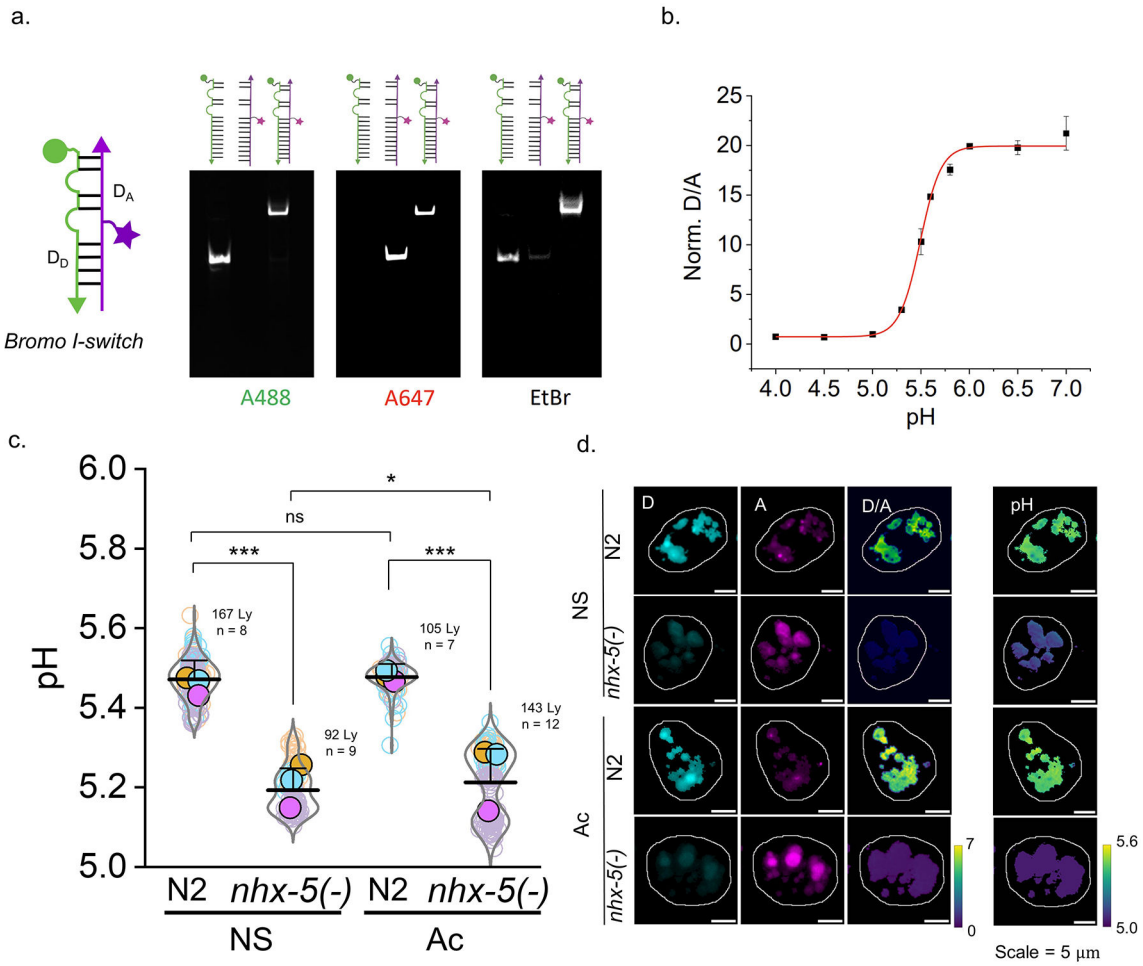

Extended Data Fig 5 |. Na^+ transporter mutants are susceptible to salt stress.

a, Brood sizes of Na^+ transporter mutants upon high salt stress. Na^+ transporter deletion mutants cannot survive 400 mM NaCl compared to WT worms. Arrows indicates condition used for lysosomal Na^+ measurement in salt stress worms is acute 200 mM (Ac worm in **d**.) **b**, Representative Na^+ heatmaps of Na^+ transporter deletion mutant worms. **c**, qRT-PCR shows that mRNA expression level of Na^+ transporters do not change appreciably upon high salt stress in N2 worms. Fold change of between Ac and Ch condition N2 worms is plotted for mRNA level of Na^+ transporters. *act-1* was used as reference gene. **d,** Lysosomal Na^+ levels of Na^+ transporter mutant worms under NS and Ac condition. Higher lysosomal Na^+ is observed in all investigated Na^+ transporter mutant worms: 9 mM in NS and 63 mM in Ac for *nhx-5(−)* worms. 24 mM in NS and 51 mM in Ac for *nhx-7(−)* worms. 34 mM in NS and 55 mM in Ac for *nhx-8(−)* worms. 25 mM in NS and 36 mM in Ac for *ncx-2(−)* worms. *P ≤ 0.05; **P ≤ 0.01; ***P ≤ 0.001; ns, no statistical significance by two sample t-test.

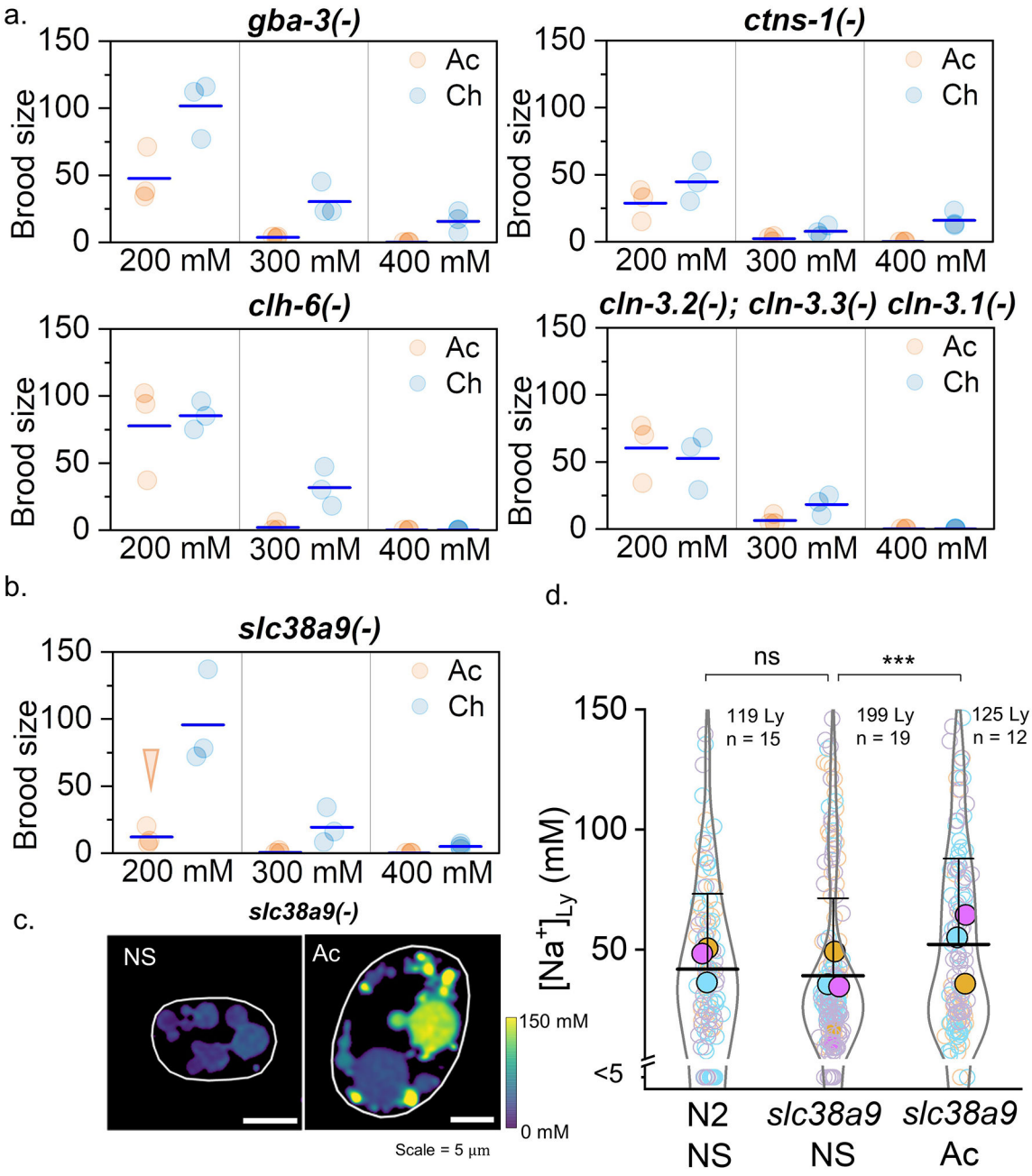

Extended Data Fig 6 |. Lysosomal pH of salt stressed worms.

a. PAGE analysis of the *I-switch*-based pH reporter module denoted *Br-I-switch*[59]. D_D strand has Alexa488N as a donor dye and D_A strand has Alexa647N as acceptor dye. b. pH calibration curve of *Br-I-switch* shows ~20 fold change of D/A signal from pH 5.0 to 6.0, with highest sensitivity near pH 5.5 which is the pH of coelomocyte lysosome[38]. c. pH measurement of single lysosome of N2 and *nhx-5(−)* worms in normal salt (NS) and acutely salt stressed (Ac) condition. nhx-5(−) has lower pH in both NS and Ac conditions. *P ≤ 0.05; **P ≤ 0.01; ***P ≤ 0.001; ns, no statistical significance by two sample t-test. d. Representative images of *Br- I-switch* in Donor (D), acceptor (A) FRET (D/A) channels and calculated pH heatmaps.

Supplementary Material

Refer to Web version on PubMed Central for supplementary material.

Acknowledgements

We thank Eduardo Perozo, Gary Ruvkun, Axel Concepcion and Ai Lin Chun for valuable discussions and input on the manuscript. We thank Christine Labno at the integrated light microscopy facilities at the University of Chicago for technical help and Tong Wu for assistance with qRT-PCR. We thank Keith Nehrke for sharing NHX-5::GFP plasmid. YK acknowledges funding from NIH grants DP1GM149751, 1R01NS112139-01A1, 1R21NS114428-01, R21HL161825-01A1, 1R01GM147197-01 (YK and RR), FA9550-19-0003 from the AFOSR, HFSP grant no: RGP0032/2022, and the Ono Pharma Foundation.

Data Availability

The raw data supporting Figures 1–4 are available for public access at Figshare: https://doi.org/10.6084/m9.figshare.23938503

References

1. Shapovalov G et al. Organelle membrane derived patches: reshaping classical methods for new targets. Sci. Rep 7, 14082 (2017). [PubMed: 29074990]
2. Nass R, Cunningham KW & Rao R Intracellular sequestration of sodium by a novel Na+/H+ exchanger in yeast is enhanced by mutations in the plasma membrane H+-ATPase. Insights into mechanisms of sodium tolerance. J. Biol. Chem 272, 26145–26152 (1997). [PubMed: 9334180]
3. Nass R & Rao R Novel localization of a Na+/H+ exchanger in a late endosomal compartment of yeast. Implications for vacuole biogenesis. J. Biol. Chem 273, 21054–21060 (1998). [PubMed: 9694857]
4. Orlowski J & Grinstein S Na+/H+ exchangers. Compr. Physiol 1, 2083–2100 (2011). [PubMed: 23733698]
5. Pedersen SF & Counillon L The SLC9A-C Mammalian Na+/H+ Exchanger Family: Molecules, Mechanisms, and Physiology. Physiol. Rev 99, 2015–2113 (2019). [PubMed: 31507243]
6. Kondapalli KC et al. Functional evaluation of autism-associated mutations in NHE9. Nat. Commun 4, 2510 (2013). [PubMed: 24065030]
7. Morrow EM et al. Identifying autism loci and genes by tracing recent shared ancestry. Science 321, 218–223 (2008). [PubMed: 18621663]
8. Pescosolido MF, Ouyang Q, Liu JS & Morrow EM Loss of christianson syndrome na+/h+ exchanger 6 (NHE6) causes abnormal endosome maturation and trafficking underlying lysosome dysfunction in neurons. J. Neurosci 41, 9235–9256 (2021). [PubMed: 34526390]
9. Fukada-Tanaka S, Inagaki Y, Yamaguchi T, Saito N & Iida S Colour-enhancing protein in blue petals. Nature 407, 581 (2000).
10. Lamason RL et al. SLC24A5, a putative cation exchanger, affects pigmentation in zebrafish and humans. Science 310, 1782–1786 (2005). [PubMed: 16357253]
11. Cang C, Bekele B & Ren D The voltage-gated sodium channel TPC1 confers endolysosomal excitability. Nat. Chem. Biol 10, 463–469 (2014). [PubMed: 24776928]
12. Cang C et al. mTOR regulates lysosomal ATP-sensitive two-pore Na(+) channels to adapt to metabolic state. Cell 152, 778–790 (2013). [PubMed: 23394946]
13. Wang X et al. TPC proteins are phosphoinositide- activated sodium-selective ion channels in endosomes and lysosomes. Cell 151, 372–383 (2012). [PubMed: 23063126]
14. Saminathan A et al. A DNA-based voltmeter for organelles. Nat. Nanotechnol 16, 96–103 (2021). [PubMed: 33139937]
15. Erecińska M & Silver IA Ions and energy in mammalian brain. Prog. Neurobiol 43, 37–71 (1994). [PubMed: 7972852]

16. Harootunian AT, Kao JP, Eckert BK & Tsien RY Fluorescence ratio imaging of cytosolic free Na+ in individual fibroblasts and lymphocytes. J. Biol. Chem 264, 19458–19467 (1989). [PubMed: 2478559]
17. Minta A & Tsien RY Fluorescent indicators for cytosolic sodium. J. Biol. Chem 264, 19449–19457 (1989). [PubMed: 2808435]
18. Steinberg BE et al. A cation counterflux supports lysosomal acidification. J. Cell Biol 189, 1171–1186 (2010). [PubMed: 20566682]
19. Leung K, Chakraborty K, Saminathan A & Krishnan Y A DNA nanomachine chemically resolves lysosomes in live cells. Nat. Nanotechnol 14, 176–183 (2019). [PubMed: 30510277]
20. Zhu H et al. Metabolomic profiling of single enlarged lysosomes. Nat. Methods 18, 788–798 (2021). [PubMed: 34127857]
21. Martin VV, Rothe A & Gee KR Fluorescent metal ion indicators based on benzoannelated crown systems: a green fluorescent indicator for intracellular sodium ions. Bioorg. Med. Chem. Lett 15, 1851–1855 (2005). [PubMed: 15780620]
22. Holmehave J, Pedersen SK, Jensen H & Ogilby PR Aarhus green: a tetrafluoro-substituted derivative of fluorescein. Arkivoc 2015, 52 (2015).
23. Rostovtsev VV, Green LG, Fokin VV & Sharpless KB A stepwise huisgen cycloaddition process: copper(I)-catalyzed regioselective “ligation” of azides and terminal alkynes. Angew. Chem. Int. Ed 41, 2596–2599 (2002).
24. Chang PV et al. Copper-free click chemistry in living animals. Proc Natl Acad Sci USA 107, 1821–1826 (2010). [PubMed: 20080615]
25. Veetil AT et al. DNA-based fluorescent probes of NOS2 activity in live brains. Proc Natl Acad Sci USA 117, 14694–14702 (2020). [PubMed: 32554491]
26. Krishnan Y, Zou J & Jani MS Quantitative imaging of biochemistry in situ and at the nanoscale. ACS Cent. Sci 6, 1938–1954 (2020). [PubMed: 33274271]
27. Surana S, Bhat JM, Koushika SP & Krishnan Y An autonomous DNA nanomachine maps spatiotemporal pH changes in a multicellular living organism. Nat. Commun 2, 340 (2011). [PubMed: 21654640]
28. Suresh B et al. Tubular lysosomes harbor active ion gradients and poise macrophages for phagocytosis. Proc Natl Acad Sci USA 118, (2021).
29. Cui C et al. A lysosome-targeted DNA nanodevice selectively targets macrophages to attenuate tumours. Nat. Nanotechnol 16, 1394–1402 (2021). [PubMed: 34764452]
30. Dan K, Veetil AT, Chakraborty K & Krishnan Y DNA nanodevices map enzymatic activity in organelles. Nat. Nanotechnol 14, 252–259 (2019). [PubMed: 30742135]
31. Surana S, Bhatia D & Krishnan Y A method to study in vivo stability of DNA nanostructures. Methods 64, 94–100 (2013). [PubMed: 23623822]
32. Ishiguro H, Steward MC, Lindsay AR & Case RM Accumulation of intracellular HCO3- by Na(+)-HCO3- cotransport in interlobular ducts from guinea-pig pancreas. J Physiol (Lond) 495 (Pt 1), 169–178 (1996). [PubMed: 8866360]
33. Saminathan A, Zajac M, Anees P & Krishnan Y Organelle-level precision with next-generation targeting technologies. Nat. Rev. Mater (2021) doi:10.1038/s41578-021-00396-8.
34. Saha S, Prakash V, Halder S, Chakraborty K & Krishnan Y A pH-independent DNA nanodevice for quantifying chloride transport in organelles of living cells. Nat. Nanotechnol 10, 645–651 (2015). [PubMed: 26098226]
35. Narayanaswamy N et al. A pH-correctable, DNA-based fluorescent reporter for organellar calcium. Nat. Methods 16, 95–102 (2019). [PubMed: 30532082]
36. Calcraft PJ et al. NAADP mobilizes calcium from acidic organelles through two-pore channels. Nature 459, 596–600 (2009). [PubMed: 19387438]
37. Ogunbayo OA et al. mTORC1 controls lysosomal Ca2+ release through the two-pore channel TPC2. Sci. Signal 11, (2018).
38. Kang Y-L et al. Inhibition of PIKfyve kinase prevents infection by Zaire ebolavirus and SARS-CoV-2. Proc Natl Acad Sci USA 117, 20803–20813 (2020). [PubMed: 32764148]

39. Prasad H & Rao R The Na+/H+ exchanger NHE6 modulates endosomal pH to control processing of amyloid precursor protein in a cell culture model of Alzheimer disease. J. Biol. Chem 290, 5311–5327 (2015). [PubMed: 25561733]
40. Yang Y & Guo Y Unraveling salt stress signaling in plants. J. Integr. Plant Biol 60, 796–804 (2018). [PubMed: 29905393]
41. Lamitina ST, Morrison R, Moeckel GW & Strange K Adaptation of the nematode Caenorhabditis elegans to extreme osmotic stress. Am J Physiol, Cell Physiol 286, C785–91 (2004). [PubMed: 14644776]
42. Urso SJ & Lamitina T The C. elegans Hypertonic Stress Response: Big Insights from Shrinking Worms. Cell. Physiol. Biochem 55, 89–105 (2021).
43. Nehrke K & Melvin JE The NHX family of Na+-H+ exchangers in Caenorhabditis elegans. J. Biol. Chem 277, 29036–29044 (2002). [PubMed: 12021279]
44. Kim J et al. NHX-5, an Endosomal Na+/H+ Exchanger, Is Associated with Metformin Action. J. Biol. Chem 291, 18591–18599 (2016). [PubMed: 27435670]
45. Collins JF et al. Molecular cloning, sequencing, tissue distribution, and functional expression of a Na+/H+ exchanger (NHE-2). Proc Natl Acad Sci USA 90, 3938–3942 (1993). [PubMed: 7683411]
46. Oberheide K, Puchkov D & Jentsch TJ Loss of the Na+/H+ exchanger NHE8 causes male infertility in mice by disrupting acrosome formation. J. Biol. Chem 292, 10845–10854 (2017). [PubMed: 28476888]
47. Assaha DVM, Ueda A, Saneoka H, Al-Yahyai R & Yaish MW The role of na+ and K+ transporters in salt stress adaptation in glycophytes. Front. Physiol 8, 509 (2017). [PubMed: 28769821]
48. Mager T, Rimon A, Padan E & Fendler K Transport mechanism and pH regulation of the Na+/H+ antiporter NhaA from Escherichia coli: an electrophysiological study. J. Biol. Chem 286, 23570–23581 (2011). [PubMed: 21566125]
49. Mindell JA Lysosomal acidification mechanisms. Annu. Rev. Physiol 74, 69–86 (2012). [PubMed: 22335796]
50. de Voer G, Peters D & Taschner PEM Caenorhabditis elegans as a model for lysosomal storage disorders. Biochim. Biophys. Acta 1782, 433–446 (2008). [PubMed: 18501720]
51. Chakraborty K, Leung K & Krishnan Y High lumenal chloride in the lysosome is critical for lysosome function. eLife 6, e28862 (2017). [PubMed: 28742019]
52. Rebsamen M et al. SLC38A9 is a component of the lysosomal amino acid sensing machinery that controls mTORC1. Nature 519, 477–481 (2015). [PubMed: 25561175]
53. Ba Q, Raghavan G, Kiselyov K & Yang G Whole-Cell Scale Dynamic Organization of Lysosomes Revealed by Spatial Statistical Analysis. Cell Rep 23, 3591–3606 (2018). [PubMed: 29925001]
54. Platt CD et al. Leucine-rich repeat containing 8A (LRRC8A)-dependent volume-regulated anion channel activity is dispensable for T-cell development and function. J. Allergy Clin. Immunol 140, 1651–1659.e1 (2017). [PubMed: 28192143]
55. López-Hernández T, Puchkov D, Krause E, Maritzen T & Haucke V Endocytic regulation of cellular ion homeostasis controls lysosome biogenesis. Nat. Cell Biol 22, 815–827 (2020). [PubMed: 32601373]
56. Jeffery J & Jörnvall H Enzyme relationships in a sorbitol pathway that bypasses glycolysis and pentose phosphates in glucose metabolism. Proc Natl Acad Sci USA 80, 901–905 (1983). [PubMed: 6405381]
57. Burg MB, Ferraris JD & Dmitrieva NI Cellular response to hyperosmotic stresses. Physiol. Rev 87, 1441–1474 (2007). [PubMed: 17928589]
58. Galluzzi L, Pietrocola F, Levine B & Kroemer G Metabolic control of autophagy. Cell 159, 1263–1276 (2014). [PubMed: 25480292]
59. Kandasamy P, Gyimesi G, Kanai Y & Hediger MA Amino acid transporters revisited: New views in health and disease. Trends Biochem. Sci 43, 752–789 (2018). [PubMed: 30177408]
60. Wang S et al. Metabolism. Lysosomal amino acid transporter SLC38A9 signals arginine sufficiency to mTORC1. Science 347, 188–194 (2015). [PubMed: 25567906]
61. Efeyan A, Comb WC & Sabatini DM Nutrient-sensing mechanisms and pathways. Nature 517, 302–310 (2015). [PubMed: 25592535]

62. Lamming DW & Bar-Peled L Lysosome: The metabolic signaling hub. Traffic 20, 27–38 (2019). [PubMed: 30306667]

63. Lord SJ, Velle KB, Mullins RD & Fritz-Laylin LK SuperPlots: Communicating reproducibility and variability in cell biology. J. Cell Biol 219, (2020).

Methods only references

1. Ellison DH & Welling P Insights into Salt Handling and Blood Pressure. N. Engl. J. Med 385, 1981–1993 (2021). [PubMed: 34788509]

2. Müller DN, Wilck N, Haase S, Kleinewietfeld M & Linker RA Sodium in the microenvironment regulates immune responses and tissue homeostasis. Nat. Rev. Immunol 19, 243–254 (2019). [PubMed: 30644452]

3. Kitada K et al. High salt intake reprioritizes osmolyte and energy metabolism for body fluid conservation. J. Clin. Invest 127, 1944–1959 (2017). [PubMed: 28414295]

4. Schindelin J et al. Fiji: an open-source platform for biological-image analysis. Nat. Methods 9, 676–682 (2012). [PubMed: 22743772]

5. Suresh B et al. Tubular lysosomes harbor active ion gradients and poise macrophages for phagocytosis. Proc. Natl. Acad. Sci 118, (2021).

6. Chakraborty K, Leung K & Krishnan Y High lumenal chloride in the lysosome is critical for lysosome function. eLife 6, e28862 (2017). [PubMed: 28742019]

7. Gholami Yarahmadi S, Sarlaki F & Morovvati S Cystinosis and two rare mutations in CTNS gene: two case reports. J. Med. Case Reports 16, 181 (2022).

8. Surana S, Bhat JM, Koushika SP & Krishnan Y An autonomous DNA nanomachine maps spatiotemporal pH changes in a multicellular living organism. Nat. Commun 2, 340 (2011). [PubMed: 21654640]

9. Nehrke K & Melvin JE The NHX Family of Na+-H+ Exchangers in Caenorhabditis elegans *. J. Biol. Chem 277, 29036–29044 (2002). [PubMed: 12021279]

10. Lamitina ST, Morrison R, Moeckel GW & Strange K Adaptation of the nematode Caenorhabditis elegans to extreme osmotic stress. Am. J. Physiol.-Cell Physiol 286, C785–C791 (2004). [PubMed: 14644776]

11. Leung K, Chakraborty K, Saminathan A & Krishnan Y A DNA nanomachine chemically resolves lysosomes in live cells. Nat. Nanotechnol 14, 176–183 (2019). [PubMed: 30510277]

12. Prasad H & Rao R Amyloid clearance defect in ApoE4 astrocytes is reversed by epigenetic correction of endosomal pH. Proc. Natl. Acad. Sci 115, E6640–E6649 (2018). [PubMed: 29946028]

13. Strømme P et al. X-linked Angelman-like syndrome caused by Slc9a6 knockout in mice exhibits evidence of endosomal-lysosomal dysfunction. Brain J. Neurol 134, 3369–3383 (2011).

14. Nasser H et al. Establishment of bone marrow-derived M-CSF receptor-dependent self-renewing macrophages. Cell Death Discov 6, 1–14 (2020).

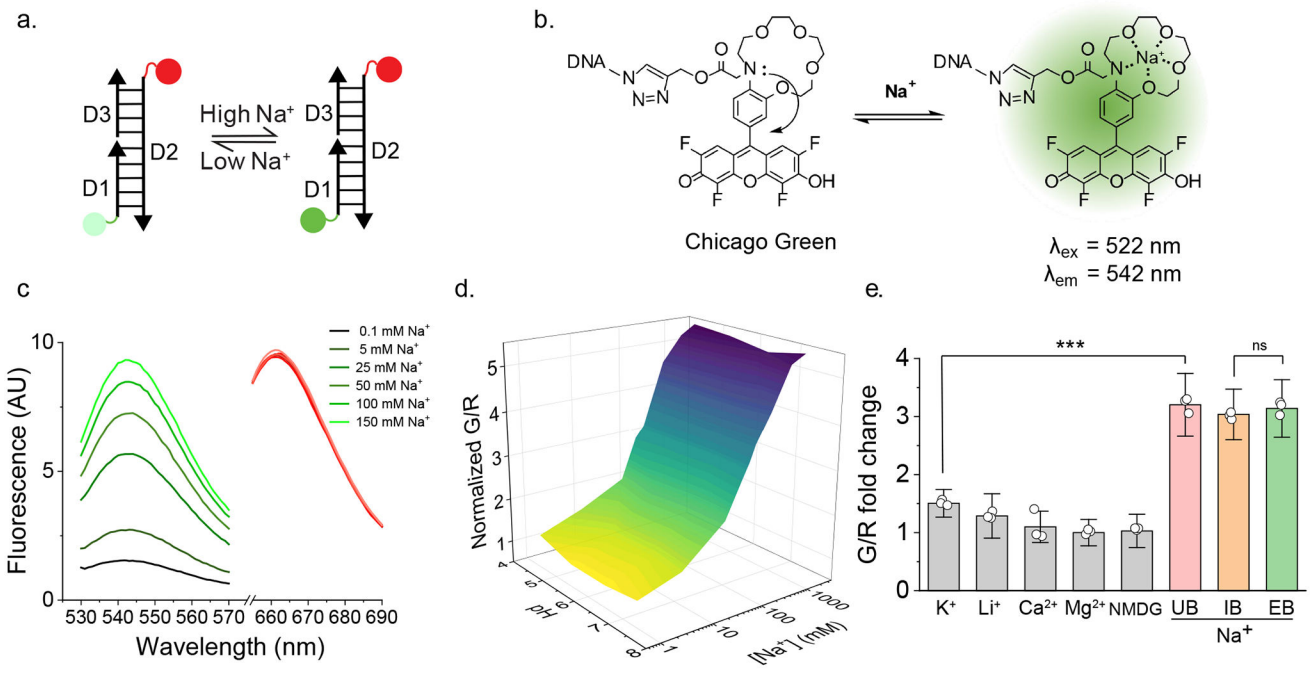

Figure 1 |. *RatiNa* is a ratiometric, pH-independent and specific reporter of Na^+.

a, Schematic of the single stranded DNA molecules comprising *RatiNa*: D1 displays a Na^+ sensing dye, Chicago Green (CG, green circle), D2 bears a reference ATTO647 fluorophore (red circle) and D3 harbors an organelle targeting motif. Na^+ binding makes CG fluoresce (dark green circle). D1 and D3 are complementary to D2. **b**, Working principle of CG. CG is quenched by the N lone pair on the aza-crown ether via photoinduced electron transfer (PET). Na^+ binding relieves PET and turns on CG fluorescence (right). **c**, *RatiNa* ratiometrically reports Na^+. Increasing Na^+ elevates fluorescence of CG (green traces) but not of ATTO647 (red traces). **d**, *In vitro* calibration profile of *RatiNa* on beads as a function of Na^+ and pH levels. Na^+ response of *RatiNa* is unaffected from pH 4.5 to 7.4. **e**, *RatiNa* responds specifically to Na^+ in the presence of other physiologically relevant cations. *RatiNa* G/R fold change in universal buffer (UB, grey) with K^+ = 145 mM; Li^+, Ca^{2+}, Mg^{2+} = 10 mM; NMDG = 0.3 M. G/R fold change with Na^+ = 145 mM in UB (pink), intracellular buffer (IB, salmon) and extracellular buffer (EB, pistachio) n = 3 independent experiments. Data are presented as mean values ± standard deviation (SD). Two sample two-tailed t-test was used for statistical analysis with no multiple comparison correction, P = 3.18E-5.

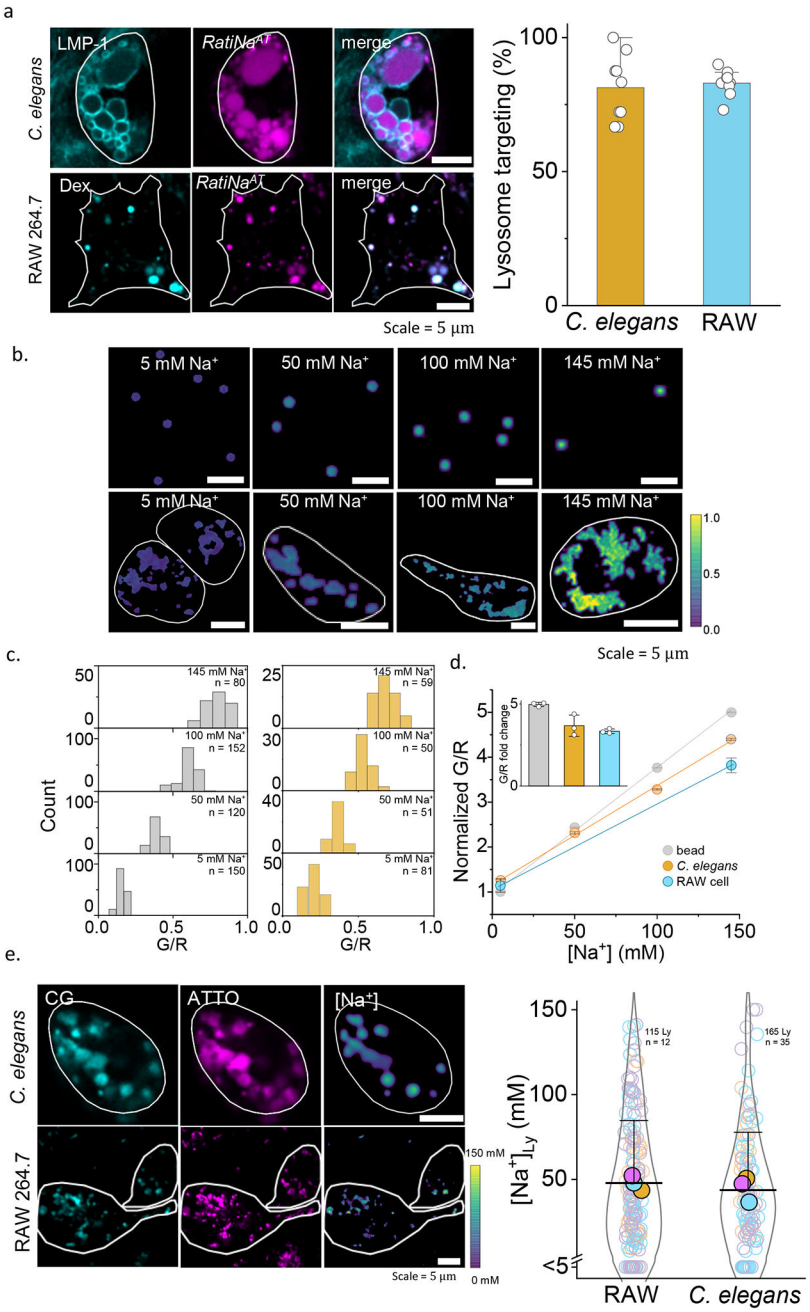

Figure 2 |. In cell and *in vivo* calibration of *RatiNa* to measure lysosomal Na^+.

a, Fluorescence images (left) show *RatiNa*^{AT} (DNA, magenta) colocalized with lysosome markers (cyan), LMP-1 in *C. elegans* and TMR-dextran (Dex) in RAW macrophages. Percentage colocalization of *RatiNa*^{AT} in lysosomes (right) in $n = 9$ coelomocytes and n = 8 RAW cells in two independent experiments. **b**, Ratiometric images of *RatiNa*^{biotin} on beads (upper panels) and *RatiNa*-labeled, Na^+ clamped *C. elegans* lysosomes (lower panels) at the indicated Na^+ levels. Cell outline shown in white. **c**, G/R values increase with increasing Na^+ on beads (grey, n = 100–150) and in worm lysosomes (ochre, n = 50–75). **d**, Linear fits of normalized G/R values of *RatiNa* as a function of [Na^+] on beads (grey), in *C.*

elegans lysosomes (ochre) and in RAW macrophages (cyan). Inset shows *RatiNa* response from 5 to 145 mM Na^+. All experiments performed in triplicate. Absolute Na^+ heatmaps of single, native, *RatiNa*-labeled lysosomes in *C. elegans* and RAW macrophages imaged in the CG (cyan) and ATTO647 (magenta) channels. Na^+ values in single lysosomes of RAW macrophages and *C. elegans* coelomocytes (n = 100–150 lysosomes from 35–50 cells). Experiments were performed in triplicate and data from each trial is colour coded. Mean value of each trial is given by a filled circle of the corresponding colour[63]. Lysosomes with Na^+ values < 5 mM are shown below the break in the Y-axis (n = 21 and 17 for RAW cells and *C. elegans*). All error bar represents mean values ± SD.

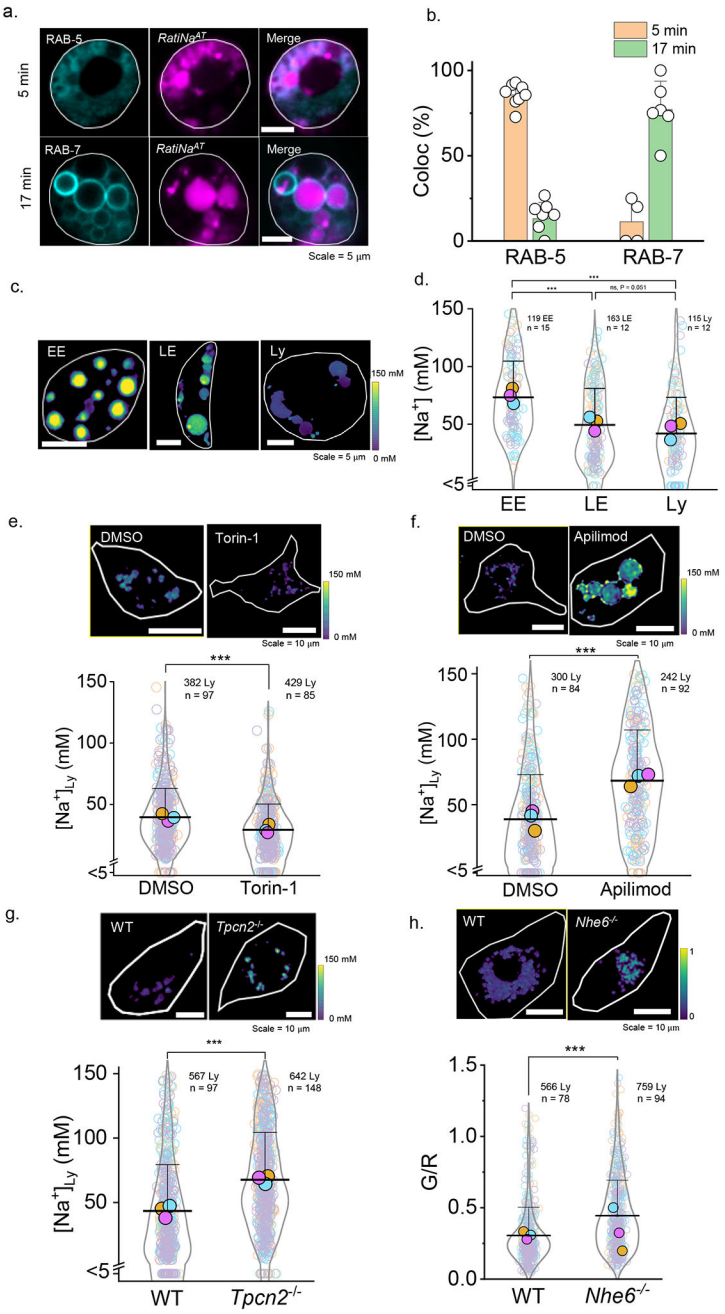

Figure 3 |. *RatiNa* captures physiological changes in organellar Na^+.

a, *RatiNa*^{AT} (magenta) colocalizes with early endosome (EE) marker, RAB-5-GFP (cyan), and late endosome (LE) marker, RAB-7-GFP (cyan), time-dependently in C. elegans coelomocytes. **b**, Quantification of colocalization between *RatiNa*^{AT} and the indicated markers at 5 min (n = 8, 4 coelomocytes) and 17 min (n = 7, 6 coelomocytes) respectively. Data are presented as mean values ± SD. **c**, *RatiNa* maps lumenal Na^+ levels at each stage of endosomal maturation in coelomocytes of N2 *C. elegans*. Images are taken at 5 min, 7 min and 40 min post microinjection. **d**, Na^+ levels decrease as endosomes mature with the biggest change from EE to LE. (n = 115–163 endosomes/lysosome from 12–15

worms). P = 2.6E-13 for EE to Ly, 7.7E-10 for EE to LE and 0.051 for LE to Ly. **e**, Pharmacological inhibition of mTOR with Torin-1 (1 mM) reduces lysosomal Na^+. P = 9.3E-11. **f**, Pharmacological inhibition of TPCN2 by apilimod (100 nM) elevates lysosomal Na^+ in RAW macrophages. Lysosomal Na^+ is elevated in **g**, RAW264.7 macrophages where *Tpcn2* is knocked out and **h**, in bone marrow derived macrophages from *Nhe6*$^{-/-}$ mice (n = 300–759 lysosomes from 84–148 cells). P = 1.3E-19, 7.5E-30, 5.5E-27 for **f, g, h**. *P ≤ 0.05; **P ≤ 0.01; ***P ≤ 0.001; ns, no statistical significance. Data in **d**-**f** are presented as mean values, error bars represent SD and two sample two-tailed t-test was used for statistical analysis assuming equal variance.

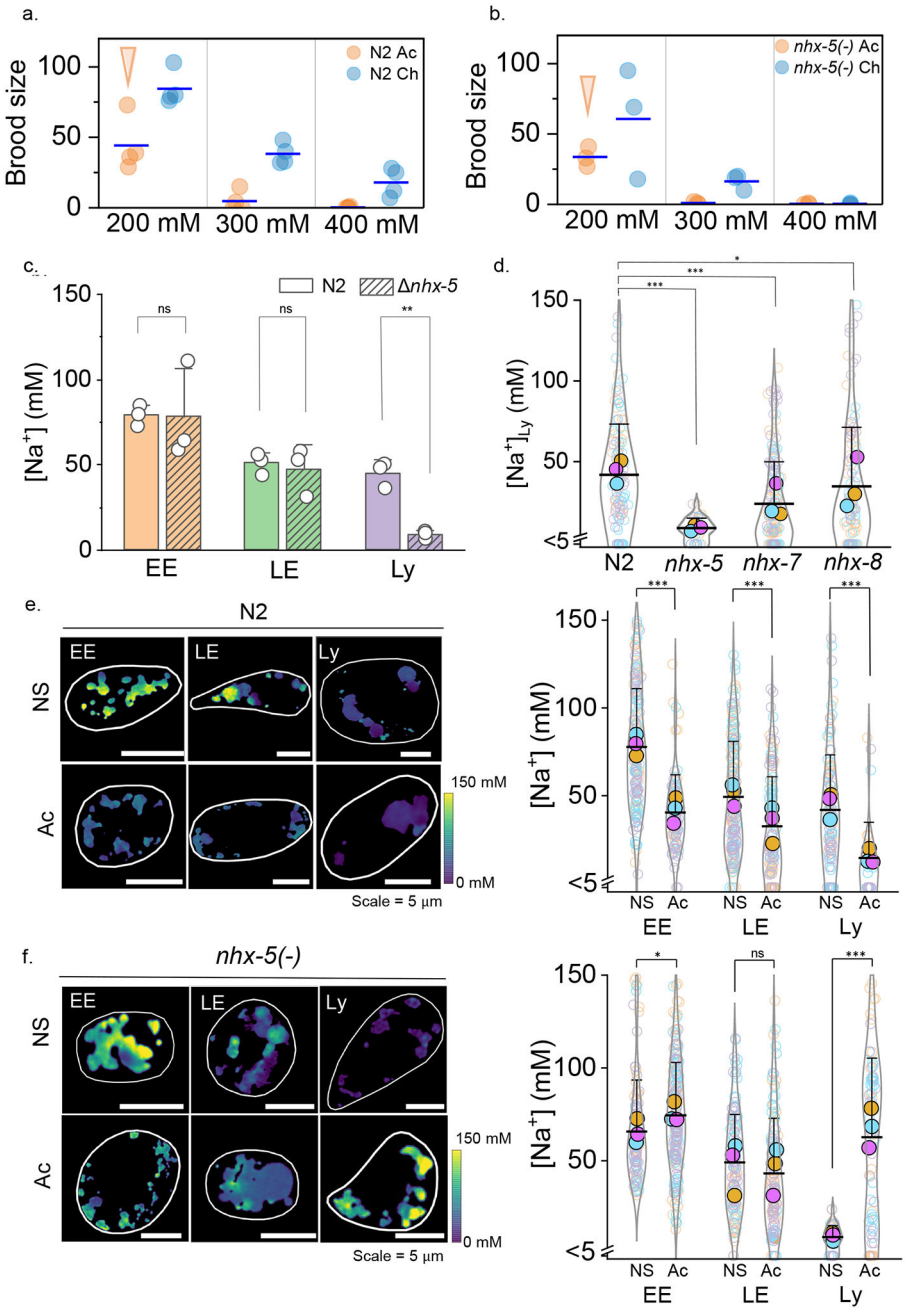

Figure 4 |. Lysosomal Na^+ transport is vital for salt adaptation in *C. elegans*.

a,b, Brood size of acutely (Ac) and chronically salt stressed (Ch) N2 and *nhx-5 (−)* worms for the indicated salt levels. Arrows indicates condition used for lysosomal Na^+ measurement in salt stressed worms is acute 200 mM **c,** Lumenal Na^+ levels at each stage of the endolysosomal pathway in N2 and *nhx-5(−)* worms in normal salt (NS). Note that *nhx-5(−)* worms show lower Na^+ levels only in lysosomes (Ly) and not in early (EE) or late endosomes (LE). P = 0.95, 0.71, 1.5E-3 for EE, LE, Ly **d**, In worms lacking the indicated *nhx* genes, Na^+ levels in single lysosomes are affected specifically by loss of *nhx-5*. Levels in n = 100–150 lysosomes from 12–16 worms. For *nhx-5 (−)* alone, n=41

lysosomes, 6 worms. P = 1.4E-10, 2.2E-7, 0.11 for N2 to *nhx-5 (−), nhx-7 (−), nhx-8 (−)*. **e, f**, Lysosomal Na^+ reduces upon chronic salt stress in N2 worms but increases in *nhx-5 (−)* worms. Lumenal Na^+ levels at each endosomal stage in normal salt (NS) and acutely (Ac) salt stressed N2 (**e**) and *nhx-5*(−) (**f**) worms. Cell outline is shown in white. All experiments were performed in triplicate and data from each trial is colour coded. Mean value of each trial given by a filled circle of the corresponding colour[58]. P = 8.9E-19, 2.7E-6, 2.2E-6 for EE, LE, Ly in N2 and P = 0.01, 0.09, 2.1E-13 for EE, LE, Ly in *nhx-5*(−) worms. For all trials, n = 130–160 organelles from 8–12 worms. Only for Ac N2 and NS *nhx-5(−)* worms, data is from n = 40 lysosomes from 6 worms. Data in **c-f** are presented as mean values, error bars represent SD and two sample two-tailed t-test was used for statistical analysis assuming equal variance.